THE EUROPEAN
PHYSICAL JOURNAL C

MSSM Higgs benchmark scenarios for Run 2 and beyond: the low tan β region

Henning Bahl[1], **Stefan Liebler**[2,a], **Tim Stefaniak**[1]

[1] DESY, Notkestraße 85, 22607 Hamburg, Germany
[2] Institute for Theoretical Physics (ITP), Karlsruhe Institute of Technology, 76131 Karlsruhe, Germany

Abstract We propose two new benchmark scenarios for Higgs-boson searches in the Minimal Supersymmetric Standard Model (MSSM). These scenarios are specifically designed for the low tan β region. A light Higgs-boson mass prediction compatible with the observed value of 125 GeV is ensured in almost the entire parameter space by employing a flexible supersymmetric (SUSY) mass scale, reaching values of up to 10^{16} GeV. The MSSM Higgs-sector predictions are evaluated in an effective field theory (EFT) framework that exhibits a Two-Higgs-Doublet-Model at the low scale. In the first scenario all SUSY particles are relatively heavy, whereas the second scenario features light neutralinos and charginos. Both scenarios are largely compatible with the most recent results from Run 2 of the LHC, and we highlight the main phenomenological features relevant for future LHC searches. In particular, we provide a detailed discussion of heavy Higgs-boson decays to neutralinos and charginos in the second scenario, and the arising collider signatures, in order to facilitate the design of dedicated LHC searches in the near future.

1 Introduction

The last free parameter in the Standard Model (SM) of particle physics, namely the mass of the Higgs boson that was discovered at the Large Hadron Collider (LHC) [1,2], was determined during Run 1 of the LHC to $M_{H^{\mathrm{SM}}}^{\mathrm{obs}} = 125.09 \pm 0.24$ GeV [3]. In addition, the Higgs-boson properties, among them the Higgs-boson couplings to the heavier SM particles and the Higgs-boson width, were found to be compatible with the SM predictions within the experimen-

tal and theoretical uncertainties [4]. This experimental information puts strong indirect constraints on beyond-the-SM (BSM) physics, which become increasingly important since no direct evidence for BSM physics has yet been found at the LHC.

One of the most compelling models of BSM physics is the Minimal Supersymmetric Standard Model (MSSM) [5–7]. Apart from associating a superpartner with each SM degree of freedom, it also extends the SM Higgs sector by a second doublet resulting in five physical Higgs states. Assuming $\mathcal{CP}$ conservation in the Higgs sector these are the light and heavy $\mathcal{CP}$-even Higgs bosons, h and H, respectively, the $\mathcal{CP}$-odd Higgs boson, A, and the charged Higgs bosons, $H^{\pm}$. Due to the underlying supersymmetry (SUSY), the MSSM Higgs sector is highly predictive. At the tree-level, all masses and couplings are determined by only two non-SM parameters. Typically, the ratio of the vacuum expectation values (vevs) of the two doublets, tan β, and the mass of the $\mathcal{CP}$-odd Higgs boson, M_A, are chosen in the $\mathcal{CP}$-conserving MSSM.

However, the tree-level predictions receive large quantum corrections. Their inclusion is especially important in the case of the SM-like Higgs-boson mass, which we assume to be the h boson in this work (see Refs. [8–12] for scenarios in which the H boson plays the role of the Higgs boson discovered at the LHC). Consequently, much work has been dedicated to the calculation of these corrections. We refer to Ref. [13] for a recent review. Through the radiative corrections a large set of parameters enter the calculation. This makes an interpretation of corresponding experimental results challenging. Consequently, benchmark scenarios have been proposed to alleviate experimental analyses and their theoretical interpretation [14–19]. Due to experimental and theoretical progress much of the parameter space of these original benchmark scenarios has been ruled out. Therefore, new benchmark scenarios, taking into account the most recent experimental limits as well as state-of-art theory predictions, have been proposed in Ref. [20].

[a] e-mail: stefan.liebler@kit.edu

In all the original benchmark scenarios as well as in the new scenarios presented in Ref. [20] the supersymmetric partners of the SM fermions (sfermions) are tied to the TeV scale. In this case, the parameter region $\tan \beta \lesssim 5$ is ruled out because the mass of the SM-like Higgs boson, M_h, is predicted to be lower than the measured value. On the other hand, experimental searches for heavy Higgs bosons decaying into bottom quarks and τ leptons [21,22] rule out the parameter space at large $\tan \beta$ up to high values of M_A beyond the TeV scale. At low $\tan \beta$ the searches for heavy Higgs bosons are much less sensitive, i.e. still allow for lower values of M_A. In this region, the Higgs bosons decay into a variety of final states, which are more difficult to handle experimentally. To re-open the parameter region of low $\tan \beta$ values, the "low-$\tan \beta$-high" scenario was proposed in Ref. [18] raising the sfermion mass scale, M_{SUSY}, up to 100 TeV in order to reach $M_h \sim 125$ GeV also for low $\tan \beta$. In case of such a large hierarchy between the electroweak scale and the sfermion scale, large logarithms, involving M_{SUSY} and e.g. the top-quark mass, appear in the calculation of M_h. These can be resummed by integrating out the sfermions at M_{SUSY} and then evolving the couplings in the effective field theory (EFT) below M_{SUSY} using renormalization group equations (RGEs) down to the electroweak scale at which the SM-like Higgs-boson mass is calculated. In the simplest approach the SM is used as EFT [23–31]. Also the "low-$\tan \beta$-high" scenario was based on this setup. However, if we assume all Higgs-boson masses to be close to the electroweak scale, i.e. below a few TeV, the Two-Higgs-Doublet Model (2HDM) has to be used as low-energy EFT to ensure a correct resummation. Such setups were published in Refs. [20,32–35]. Those works show that a substantial part of the parameter space in the "low-$\tan \beta$-high" scenario yields a prediction for the light Higgs-bosons mass, M_h, which is much lower than the measured value and hence the "low-$\tan \beta$-high" scenario is meanwhile ruled out. It is the goal of this paper to define new scenarios valid at low values of $\tan \beta$ in the framework of a low-energy 2HDM.

Moreover, this region of low $\tan \beta$ is the region of validity of the hMSSM [36–38], an approximation of the MSSM Higgs sector, which assumes that the dominant correction to Higgs boson masses and mixing have a common origin: they stem from the top-quark and its SUSY partners, the stops, entering a single element of the neutral $\mathcal{CP}$-even Higgs-boson mass matrix only. As indicated this assumption is only valid at low values of $\tan \beta$ and in addition for low values of μ/M_{SUSY}, and then allows to trade the loop corrections as a function of the light Higgs boson mass M_h (for specific values of M_A and $\tan \beta$) such that the explicit dependence of the Higgs masses and mixing on the SUSY parameters can be ignored. For low $\tan \beta$ the original hMSSM approach is known to approximate Higgs masses and mixing quite well, see e.g. Refs. [18,33,39], though for the Higgs-boson cou-

plings, entering e.g. the important decay $H \rightarrow hh$, further refinements [40] are needed. In comparison with our suggested scenarios the quality of the hMSSM approximation and its region of validity can be tested. As a first step, we compare the $\mathcal{CP}$-even Higgs-boson mixing angle, α, and the heavy $\mathcal{CP}$-even Higgs-boson mass, M_H, between the two approaches, but leave a discussion of more elaborate quantities, including the prediction of the $H \rightarrow hh$ partial width, to future work.

We shall define two scenarios: One scenario in which all non-2HDM states are decoupled and one featuring light neutralinos and charginos, to which we refer as electroweakinos. The first scenario resembles the M_h^{125} scenario, the other the $M_h^{125}(\tilde{\chi})$ scenario, which were defined in Ref. [20]. In order to allow for $M_h \sim 125$ GeV also at low $\tan \beta$, a very high sfermion mass scale of up to 10^{16} GeV is needed. We employ a state-of-the-art calculation of the Higgs-boson masses and branching ratios using a yet unpublished version of `FeynHiggs` [24,28,30,41–45]. This version implements the results of Ref. [46]: The effective 2HDM (and a 2HDM+EWinos) as EFT below the sfermion scale includes full two-loop renormalization group equations as well as full one-loop and partial two-loop threshold corrections. This EFT calculation is combined with a state-of-the-art fixed-order calculation. For more details we refer to Ref. [46]. We obtain the production cross sections of the neutral Higgs bosons from `SusHi` [47,48] for gluon fusion and re-weight matched predictions published in Refs. [49–52] for bottom-quark associated production. We explore the known experimental constraints on the MSSM Higgs sector using `HiggsBounds` [53–56] and `HiggsSignals` [57].

The paper is set up as follows: We explain our theoretical setup in detail in Sect. 2. We proceed with an explanation of the experimental constraints in Sect. 3. Finally we define and discuss our two benchmark scenarios in Sect. 4 including a first comparison with the hMSSM approach and conclude thereafter.

2 Theory setup

In this section, we provide details about the calculation of the Higgs-boson masses and branching ratios as well as of the Higgs-boson production cross sections.

2.1 Higgs-boson masses and branching ratios

For the calculation of the Higgs-boson properties (masses and branching ratios), we rely on the code `FeynHiggs`. Since the scenarios presented in this work include a large hierarchy between the scale of non-SM-like Higgs bosons and scalar fermions, we use a yet not public `FeynHiggs`

version[1] which implements a low-energy 2HDM as well as a low-energy 2HDM+EWinos as effective field theories [46],[2] which is merged with a one-loop diagrammatic fixed-order calculation [44,60–62]. The two-loop diagrammatic fixed-order corrections implemented in FeynHiggs are switched off, see below.

For future reference, we list the FeynHiggs flags set to obtain the result presented in this work,

mssmpart = 4,　higgsmix = 2,　p2approx = 4,

looplevel = 1, loglevel = 4,　runningMT = 1,

botResum = 1,　tlCplxApprox = 0.

Setting loglevel = 4 enables the 2HDM as low-energy theory. This flag choice is not yet available in the most recent public FeynHiggs version 2.14.3, but will become available in an upcoming version.

In order to provide a numerical stable prediction for very high SUSY scales of up to 10^{16} GeV, the code has to be compiled using quadruple precision. To improve numerical stability, also an improved solving algorithm for the renormalization group equation was implemented. In addition, we have to deactivate the diagrammatic two-loop corrections to the Higgs-boson self-energies, which are numerically unstable in this parameter region even in case of quadruple precision. Note that two-loop terms which are not suppressed by the SUSY scale, re-enter via the EFT calculation.[3] The missing suppressed terms are completely negligible. For the same reason, the used one-loop Higgs-boson self-energies are expanded in the limit of large sfermion masses. We want to point out that with this FeynHiggs configuration $\tan\beta$ is defined in the 2HDM at the scale M_A. In contrast, in the benchmark scenarios defined in Ref. [20], $\tan\beta$ is evaluated at the scale of the top-quark mass, M_t.

We outlined the history of EFT calculations of the Higgs-boson mass already in the introduction. Apart from FeynHiggs there are two other codes implementing the 2HDM as low-energy EFT. These are MhEFT [33] and FlexibleSUSY [34,63].[4] Among these codes, the prediction of the light Higgs-boson mass, M_h, is in good agreement. A comparison of these codes with FeynHiggs, however, yields discrepancies of a few GeV in the prediction of M_h in the region of $M_A \sim 200$ GeV, $\tan\beta \sim 1$, $\mu \sim 200$ GeV and $M_{\rm SUSY}$ above 10^{10} GeV, where FeynHiggs predicts

higher M_h values.[5] Thus using the other codes instead could exclude parts of this region of the parameter space by a too low prediction of M_h. As we will show in Sect. 4, this region is already excluded by the Higgs-boson signal-strength measurements. For higher $\tan\beta$ or M_A values $M_{\rm SUSY}$ can be adjusted to get $M_h \sim 125$ GeV without changing the low-energy phenomenology. Therefore, while it will be still important to understand the observed discrepancy between the FeynHiggs and MhEFT/FlexibleSUSY predictions, the outcome of this discussion will hardly affect the phenomenology of the scenarios presented in this work.

2.2 Production cross sections

For the calculation of the gluon-fusion cross sections of the neutral Higgs bosons we employ SusHi 1.7.0 [47,48], which we directly link to FeynHiggs at quadruple precision. We take into account the Higgs-boson mixing by implementing the full **Z** matrix as explained in Ref. [64]. The **Z** matrix relates the tree-level mass eigenstates to the external physical states and is calculated by FeynHiggs including a resummation of large logarithms by the means of the EFT calculation [44,65,66]. SusHi includes top- and bottom-quark contributions at next-to-leading order (NLO) [67,68] and for the top-quark contribution adds next-to-NLO (NNLO) effects in the heavy-quark effective theory [69–73] as well as next-to-NNLO (N^{3}LO) contributions, which additionally exploit a threshold expansion [74–76]. The latter N^{3}LO contributions are only taken into account for the light SM-like Higgs boson to match the precision of the LHC-HXSWG gluon-fusion cross section in the SM, see Ref. [77], except from NNLO top-quark mass effects. The N^{3}LO contribution in the threshold expansion closely matches the exact result published in Ref. [78]. We also include two-loop electroweak corrections from light quarks as discussed in Refs. [79,80]. On the other hand, we omit corrections from SUSY particles to gluon fusion, both explicit in the amplitude and through Δ_b corrections. This is justified from the fact that those contributions quickly decouple for high SUSY masses as employed in this work. Their inclusion would induce numerical instabilities due to the high SUSY masses. Keeping μ at the electroweak scale and fixing the gluino mass, M_3, to 2.5 TeV, this statement also applies to the dominant Δ_b corrections. We make use of the parton distribution functions (PDF) named PDF4LHC15_nlo_mc and PDF4LHC15_nnlo_mc [81] and choose half of the Higgs-boson mass as central renormalization and factorization scale.

---

[1] Until its official release the employed version of FeynHiggs can be obtained from the authors upon request.

[2] We corrected the renormalization group equations used in Ref. [46] according to the findings of Refs. [58,59]. The numerical effect is negligibly small.

[3] This includes corrections involving only 2HDM particles.

[4] They do provide predictions for the Higgs-boson masses but not (yet) for their branching ratios.

---

[5] In contrast to the other codes, the EFT calculation implemented in FeynHiggs takes into account all effective couplings as well as full one-loop threshold corrections, see Ref. [46] for more details. This may be the origin of the observed numerical discrepancies.

Instead of employing "Santander-matched" cross sections [82] for the production of neutral Higgs bosons through bottom-quark annihilation, we follow the recommendation of the LHC-HXSWG [77] and use the results based on soft-collinear effective theory [51,52] and the "fixed order plus next-to-leading log" (FONLL) approach [49,50], which both yield identical cross sections. They are based on the cross sections obtained in the five-flavor scheme [83] and in the four-flavor scheme [84,85]. We re-weight the cross section of the SM Higgs boson proportional to the squared bottom-quark Yukawa coupling both for the $\mathcal{CP}$-even and $\mathcal{CP}$-odd Higgs bosons and omit corrections proportional to the top-quark Yukawa coupling.

For a detailed discussion of the theoretical uncertainties of neutral Higgs-boson production in the MSSM we refer to Ref. [86]. We obtain theoretical uncertainties for gluon fusion and bottom-quark annihilation in the same way as discussed in Ref. [46], in summary: For gluon fusion we include the renormalization-scale uncertainty, which is calculated analytically from 100 scale choices between half and twice the central scale choice following the approach discussed in Ref. [48]. The difference between the maximal and minimal cross section is used as symmetric uncertainty. The factorization-scale uncertainty is subdominant and not further considered. We take into account relative PDF and α_s uncertainties obtained as a function of the Higgs-boson mass for a SM Higgs boson and for a 2HDM $\mathcal{CP}$-odd Higgs boson at $\tan\beta = 1$, which we employ for $\mathcal{CP}$-even and the $\mathcal{CP}$-odd Higgs bosons, respectively. The absolute renormalization-scale and PDF+α_s uncertainties are added in quadrature. For bottom-quark associated production we use the absolute uncertainties provided by the LHC-HXSWG both for $\mathcal{CP}$-even and $\mathcal{CP}$-odd Higgs bosons, which include renormalization- and factorization-scale uncertainties, uncertainties related to the value of the bottom-quark mass and the bottom-quark matching scale and PDF+α_s uncertainties.

Lastly we employ cross sections for charged Higgs-boson production according to the recommendation of the LHC-HXSWG, which is based upon Refs. [87–91]. This in particular includes cross sections for charged Higgs bosons in the mass window of $145 - 200$ GeV at a center-of-mass energy of 13 TeV.

3 Experimental constraints

Searches for additional Higgs bosons at the LHC, as well as the signal-strength measurements of the observed Higgs boson at the LHC, already constrain part of the parameter space of our benchmark scenarios. These constraints are tested in our analysis with the codes `HiggsBounds` [53–56] and `HiggsSignals` [57], respectively. We follow the

same procedure as in Ref. [20], which we summarize briefly in the following.

3.1 Constraints from LHC searches for additional Higgs bosons

The program `HiggsBounds` tests each parameter point against the 95% C.L. cross-section limits from neutral and charged Higgs boson searches at the LEP, Tevatron and LHC experiments. It turns out, however, that only the LHC Higgs searches are important in our benchmark scenarios. The code follows a well-defined statistical procedure when applying these constraints: in a first step, it determines the most sensitive experimental search for each Higgs boson in the model (as judged by the expected limit); in the second step only the observed upper limit of this most sensitive search is compared to the model-predicted signal rate, and the model is regarded as excluded if the predicted rate exceeds the upper limit. We refer to Refs. [53–56] for more details.

The latest version of `HiggsBounds`, `5.3.0beta`, includes results from the following LHC searches relevant to our scenarios: searches for heavy Higgs bosons decaying to $\tau^+\tau^-$ pairs by ATLAS [21] and CMS [22] using about $36\,\mathrm{fb}^{-1}$ of Run-2 data, as well as the CMS results from Run 1 [92]; ATLAS [93,94] and CMS [95,96] searches during Run-1 and Run-2 for a heavy scalar decaying to a Z-boson pair; Run-2 searches by ATLAS [97] and CMS [98–101] for a heavy scalar decaying to a pair of SM-like Higgs bosons. The most relevant charged Higgs-boson searches included in `HiggsBounds` are searches for top-quark associated $H^\pm$ production, with subsequent decays to $\tau\nu$ [102–105] or tb [102,106,107] pairs.

We estimate the theoretical uncertainty in our determination of the excluded regions by re-evaluating the excluded region with `HiggsBounds` for (*i*) a most conservative and (*ii*) a least conservative variation of the gluon-fusion and bottom-quark annihilation cross sections by their estimated uncertainties, see Sect. 2.2 and Ref. [46].

3.2 Constraints from the Higgs boson observed at the LHC

We test the compatibility with the observed Higgs-boson signal rates with the program `HiggsSignals` (version `2.2.1beta`). The program includes the combined LHC Run-1 ATLAS and CMS measurements of the Higgs-boson signal strengths [4] as well as recent measurements during LHC Run-2 that became available in mid-2018, with around $36\,\mathrm{fb}^{-1}$ of integrated luminosity per experiment [108–124]. The program evaluates a χ^2 value for each parameter point using in total 100 individual signal-rate measurements. Using this χ^2 value, we perform an (approximate) log-likelihood ratio test for model discrimination as follows: within the considered two-dimensional benchmark plane, we determine the

parameter point with minimal χ^2 value, $\chi^2_{\min}$, and regard all parameter points with $\Delta\chi^2 \equiv \chi^2 - \chi^2_{\min} \leq 6.18$ to be consistent at the 2σ level with the best-fit hypothesis (and, hence, with the observed Higgs rates). We remark that, in both of our proposed benchmark scenarios, the best fit point is found far in the decoupling limit ($M_A \gg M_Z$), where the model provides essentially as good a fit to the observed Higgs rates as the SM.

4 Benchmark scenarios

We subsequently explain our parameter choices and present two benchmark scenarios for low values of $\tan\beta$ between 1 and 10, based on the previously discussed EFT setup employing a very heavy colored SUSY spectrum. Both are inspired by two scenarios presented in Ref. [46], which work with a TeV-scale colored SUSY spectrum and are thus only valid at higher values of $\tan\beta$.

4.1 Input parameters

Following the recommendation of the LHC-HXSWG in Ref. [77], we make use of the following SM input parameters:

$$m_t^{\text{pole}} = 172.5 \text{ GeV}, \quad \alpha_s(M_Z) = 0.118,$$
$$G_F = 1.16637 \times 10^{-5} \text{ GeV}^{-2},$$
$$m_b(m_b) = 4.18 \text{ GeV}, \quad M_Z = 91.1876 \text{ GeV},$$
$$M_W = 80.385 \text{ GeV}. \tag{1}$$

The other lepton and quarks masses only have a minor influence on the Higgs-sector observables. Therefore, we stick to the default values of FeynHiggs. There, however, is a strong dependence of the light Higgs-boson mass, M_h, on the value of the employed top-quark pole mass. The value recommended by the LHC-HXSWG is below the current world average of $173.21 \pm 0.51 \pm 0.71$ GeV [125]. In the scenarios considered here, a change of the top-quark pole mass of 0.7 GeV would imply a change of ~ 0.8 GeV in the prediction for M_h.

To fix the SUSY parameters, we choose to set all scalar fermion soft-SUSY breaking masses equal to a common scale M_{SUSY}. In both scenarios, presented here, M_{SUSY} will be adjusted at each point in the (M_A, $\tan\beta$) plane such that $M_h \sim$ 125 GeV is reached.[6] We, however, do not allow M_{SUSY} to be larger than 10^{16} GeV. The minimal value of M_{SUSY} in both benchmark scenarios is ~ 6 TeV, when restricting to values of $\tan\beta$ between 1 and 10 and M_A to be less than 2 TeV.

In addition, in both scenarios, we choose for the gluino mass and the third-generation soft-SUSY breaking trilinear couplings,

$$M_3 = 2.5 \text{ TeV}, \quad A_t = A_b = A_\tau = 0, \tag{2}$$

respectively. Typically, large A_t values are chosen to reach $M_h \sim 125$ GeV for low M_{SUSY} values. In the scenarios considered here, we are interested most in the region of low $\tan\beta$ and low M_A. In this region, very high M_{SUSY} values of up to 10^{16} GeV are needed to reach $M_h \sim 125$ GeV. For such high values of M_{SUSY}, there is only a mild dependence of the prediction for M_h on the size of the stop mixing. And due to theoretical fine-tuning arguments, low A_t values are preferred in case of a TeV-scale M_3 and TeV-scale electroweakinos. Fixing M_3 to 2.5 TeV, the gluino mass is safely above current bounds from direct searches [126–131].

4.2 $M_{h,\text{EFT}}^{125}$ scenario

The first benchmark scenario we propose is the $M_{h,\text{EFT}}^{125}$ scenario. All SUSY particles are chosen to be heavy. Consequently, all MSSM Higgs boson collider observables are only mildly affected by SUSY particles and the phenomenology is very similar to that of a type-II 2HDM. This scenario serves as a phenomenologically viable extension of the M_h^{125} scenario presented in Ref. [20] to low $\tan\beta$ values.[7] Hence, we choose the same Higgsino, bino and wino mass parameters,

$$\mu = 1 \text{ TeV}, \quad M_1 = 1 \text{ TeV}, \quad M_2 = 1 \text{ TeV}, \tag{3}$$

respectively. The other input parameters are fixed according to Eq. (2). With this parameter choice, the scenario is similar to the old "low-$\tan\beta$-high" scenario [18], where the electroweakinos were also chosen to have masses around the TeV scale. The $M_{h,\text{EFT}}^{125}$ scenario is a concrete realization of an MSSM scenario, which fulfills the assumptions used in the hMSSM approach [36,38,39]: It is defined in the region of interest, i.e. low $\tan\beta$ and low M_A, where for low μ/M_{SUSY} the dominant corrections to the Higgs-boson mass matrix stem from a single element in the (2×2) $\mathcal{CP}$-even Higgs-boson mass matrix. Therefore it is a perfect candidate for a more detailed comparison of remaining discrepancies in Higgs-boson mass and mixing predictions as well as Higgs-boson self-couplings and Higgs-to-Higgs decays, see e.g. Ref. [18]. Those discrepancies could reveal potential limitations of the hMSSM approach. We present a comparison of the heavy $\mathcal{CP}$-even Higgs-boson mass, M_H, and the Higgs-boson mixing angle, α, in the following subsection.

In Fig. 1 we present the current constraints on the $M_{h,\text{EFT}}^{125}$ scenario in the (M_A, $\tan\beta$) parameter plane. As described above, the SUSY mass scale, M_{SUSY}, is adjusted at every point in order to obtain $M_h \simeq 125$ GeV throughout the parameter plane. In the *gray area*, however, $M_h < 122$ GeV, since M_{SUSY} would have to be raised above our imposed

---

[6] Tables listing the M_{SUSY} values are available as auxiliary material to this manuscript.

[7] Low values of $\tan\beta$ in an effective 2HDM are also well motivated from flavor and stability constraints [132].
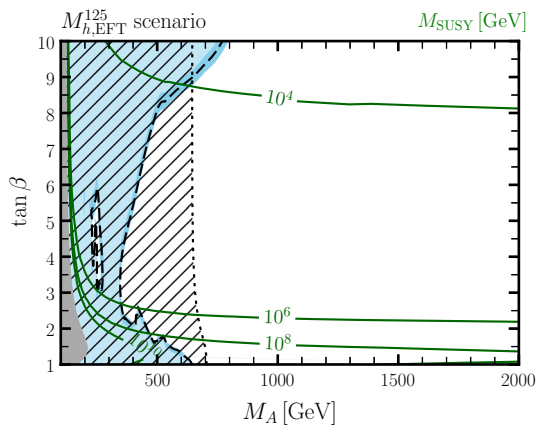
Fig. 1 The $M_{h,\text{EFT}}^{125}$ benchmark scenario shown in the $(M_A, \tan\beta)$ plane. The *green solid contour lines* indicate the required SUSY scale. The *black dotted line* and *hatched area* marks the parameter space which is disfavored at the 2σ level by the measured Higgs-boson signal rates. The *blue region* with the *black dashed edge* is excluded at the 95% C.L. by LHC searches for additional Higgs bosons (the *dark blue band* shows how the theoretical rate uncertainty affects the exclusion). The *gray area* is excluded because the mass of the SM-like Higgs boson h is below 122 GeV

upper limit of 10^{16} GeV in order to obtain large M_h values.[8] This part of the parameter space is therefore excluded.

Direct searches at the LHC for non-SM-like Higgs bosons exclude the *blue region* in Fig. 1, as determined with `HiggsBounds`. The *dark blue band* indicates the theoretical uncertainty of the exclusion, obtained by varying the cross section of H and A production in gluon fusion and in association with a bottom-quark pair, as described in Sects. 2.2 and 3.1. For $\tan\beta$ values larger than around $3-4$, the most important search channel is $gg/b\bar{b} \rightarrow H/A \rightarrow \tau^+\tau^-$. The CMS analysis [22] is slightly more sensitive than the ATLAS analysis [21] and excludes M_A values of $\lesssim 400$ (750) GeV for $\tan\beta \sim 5$ (10), except for a small parameter region at $M_A \sim 250$ GeV and $\tan\beta \sim 3-6$. In this region, LHC searches for $pp \rightarrow H \rightarrow ZZ$ show similar or even higher sensitivity. The applied ATLAS search limit [94], however, exhibits some statistical fluctuations in this region, leading to the observed hole (and tiny spike) in the exclusion.[9] At lower $\tan\beta$ values direct searches for $pp \rightarrow H \rightarrow hh$ become important. Currently, the most sensitive final state of this process is $\tau^+\tau^-b\bar{b}$, with the CMS search [100] being more sensitive for lower masses, $M_A < 420$ GeV, and the ATLAS search [97] for higher masses up to $M_A \sim 500$ GeV.[10] Beyond $M_A \sim 500$ GeV, at very low $\tan\beta$ val-

ues, the exclusion arises from the CMS combination of $H \rightarrow hh \rightarrow b\bar{b}\gamma\gamma$, $b\bar{b}\tau^+\tau^-$, $b\bar{b}b\bar{b}$, $b\bar{b}VV$ ($V = W, Z$) search results [101]. Part of this region (at very small $\tan\beta \sim 1$) is furthermore constrained by charged Higgs boson searches in the $pp \rightarrow tbH^\pm \rightarrow tb(tb)$ channel [107].

The *hatched region* of Fig. 1 is disfavored at the 2σ level by the SM-like Higgs-boson rate measurements at the LHC, as evaluated by `HiggsSignals`. Its boundary is located at around $M_A \simeq 650$ GeV and depends only mildly on $\tan\beta$. Lower M_A values are excluded as the coupling of the light Higgs boson to bottom quarks is enhanced with respect to the SM prediction. At larger M_A values this coupling approaches the SM value, as expected in the decoupling limit. At very small $\tan\beta$, the Higgs rate measurements exclude values up to $M_A \simeq 700$ GeV due to a suppression of the light Higgs-boson gluon-fusion cross section by a few percent. This originates from a slight suppression of the light Higgs-boson coupling to top quarks induced by higher-order corrections to the external Higgs leg (accounted for by employing the **Z**-matrix).

The *green contours* in Fig. 1 indicate the M_{SUSY} values required to reach $M_h \simeq 125$ GeV. While only moderate M_{SUSY} values of up to 10^4 GeV are required for $\tan\beta \gtrsim 8$, much higher values up to around 10^8 GeV are needed for $\tan\beta \gtrsim 1.5$. Moreover, if M_A is below 500 GeV, M_{SUSY} has to be raised to very large values of 10^{10} GeV and higher. As mentioned above, for very low $M_A \lesssim 200$ GeV, M_{SUSY} would have to be raised above 10^{16} GeV to obtain $M_h \geq 122$ GeV, a region that we disregard in our work.

We further explore the required SUSY scale in Fig. 2, which shows $M_h = 125$ GeV contours (*solid*) as a function of M_{SUSY} and $X_t^{\overline{\text{DR}}}/M_{\text{SUSY}}$ (with $X_t = A_t - \mu/\tan\beta$) for $\tan\beta = 1$ (*blue*), $\tan\beta = 2.5$ (*red*) and $\tan\beta = 10$ (*green*) and $M_A = 1$ TeV. Note that in the $M_{h,\text{EFT}}^{125}$ bench-
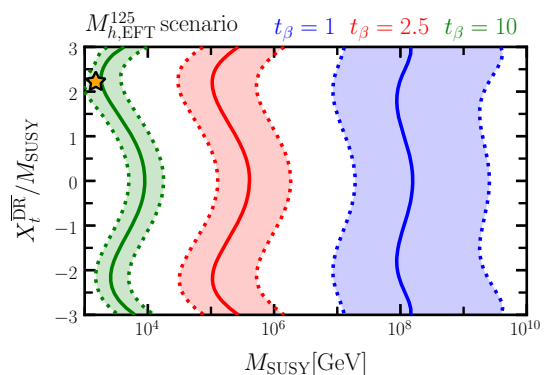
---

[8] Outside of the *gray region*, the prediction for M_h quickly increases from $M_h = 122$ GeV to $M_h = 125$ GeV.

[9] Note that a proper combination of experimental results by the LHC collaborations would presumably close the gap in the exclusion.

[10] The transition between the two analyses results in the spike observed in the exclusion region at $M_A \sim 420$ GeV and $\tan\beta \sim 2.5$.

Fig. 2 Contour lines of $M_h \simeq 125$ GeV (*solid*) and $M_h \simeq 122, 128$ GeV (*dashed*) as a function of M_{SUSY} and $X_t^{\overline{\text{DR}}}/M_{\text{SUSY}}$, for $\tan\beta = 1$ (*blue*), $\tan\beta = 2.5$ (*red*) and $\tan\beta = 10$ (*green*). M_A is fixed to 1 TeV. All remaining parameters are as in the $M_{h,\text{EFT}}^{125}$ scenario. The *orange star* marks the approximate position of the M_h^{125} scenario [20]

mark scenario, as defined in Eqs. (2) and (3), $X_t^{\overline{\mathrm{DR}}}/M_{\mathrm{SUSY}}$ is almost zero. Clearly, the needed M_{SUSY} value strongly depends on the chosen $\tan\beta$ value. While for $\tan\beta = 10$ values of $\mathcal{O}(10^3\,\mathrm{GeV})$ are sufficient, for $\tan\beta = 1$ values of $\mathcal{O}(10^8\,\mathrm{GeV})$ are needed. We also observe that for high SUSY scales there is only a mild dependence on $X_t^{\overline{\mathrm{DR}}}/M_{\mathrm{SUSY}}$. This behavior reflects the decrease of the strong gauge coupling and the top-quark Yukawa coupling, which multiply the dominant threshold corrections between the full MSSM and the EFT below the SUSY scale involving $X_t^{\overline{\mathrm{DR}}}/M_{\mathrm{SUSY}}$, with rising M_{SUSY}. Therefore, at low $\tan\beta$ values, choosing a high value of $|X_t^{\overline{\mathrm{DR}}}/M_{\mathrm{SUSY}}|$ does not allow to significantly lower the required SUSY scale. The *dashed lines* mark the contours of $M_h = 122\,\mathrm{GeV}$ and $M_h = 128\,\mathrm{GeV}$, indicating the allowed region when taking into account a simple global theoretical uncertainty estimate of 3 GeV on the Higgs mass calculation [43,133]. The broadening of the corresponding colored band with rising M_{SUSY} corresponds to a growing uncertainty in the deduction of the required SUSY scale.

For comparison, we also show in Fig. 2 the approximate position of the M_h^{125} scenario of Ref. [20] in the considered parameter plane (*orange star*). In the M_h^{125} scenario the masses of the third-generation squarks is set to 1.5 TeV. A large stop mixing parameter of $X_t^{\mathrm{OS}} = 2.8\,\mathrm{GeV}$ is needed to obtain $M_h \simeq 125\,\mathrm{GeV}$.[11]

We explore the decays of the $\mathcal{CP}$-even H and $\mathcal{CP}$-odd A bosons in Fig. 3 in the parameter region of $M_A \leq 1$ TeV. The *left panel* shows the branching ratios of the H boson decays into a pair of light Higgs bosons, $H \to hh$ (*blue contours*), and into a pair of top quarks, $H \to t\bar{t}$ (*green contours*). At low values $M_H \lesssim 2M_t$, the decay $H \to hh$ can reach a branching ratio of more than 50% (at low $\tan\beta$). It mostly competes with the decays $H \to VV$ ($V = W, Z$) in this mass regime. Once M_A is raised above the kinematic threshold for the $H \to t\bar{t}$ decay, $M_H \gtrsim 2M_t$, the decay $H \to t\bar{t}$ becomes the dominant mode and suppresses the $H \to hh$ and $H \to VV$ decays. In the unexcluded region ($M_A \gtrsim 650$ GeV), the branching ratio for $H \to hh$ drops below 10%, while the decay $H \to t\bar{t}$ can reach values above 90% for low $\tan\beta$. If $\tan\beta$ is increased the H boson coupling to top quarks becomes suppressed while its coupling to bottom quarks and tau leptons becomes enhanced, such that the decay $H \to b\bar{b}$ eventually becomes dominant. The *right panel* of Fig. 3 shows the branching ratios of the A boson decays into a Z boson and a h boson, $A \to Zh$ (*blue contours*), and into a top-quark pair, $A \to t\bar{t}$ (*green contours*). We observe a qualitatively similar behavior as for the H decays. However, below the top-quark pair production

---

[11] In the M_h^{125} scenario, the OS scheme is used for the renormalization of the stop parameters. We converted the OS parameters at the one-loop level to the $\overline{\mathrm{DR}}$ scheme to obtain the approximate position in the $(M_{\mathrm{SUSY}}, X_t^{\overline{\mathrm{DR}}}/M_{\mathrm{SUSY}})$ plane shown in Fig. 2.

threshold, the $A \to Zh$ decay competes against the decay into a bottom-quark pair, $A \to b\bar{b}$, which is dominant for $\tan\beta \gtrsim 3$. Beyond its kinematic threshold, $M_A \simeq 2M_t$, the decay $A \to t\bar{t}$ quickly becomes dominant, and the decay $A \to Zh$ is negligible. In this mass regime we therefore expect that upcoming dedicated LHC searches for heavy Higgs bosons decaying to top-quark pairs, see Ref. [134] for a Run-1 analysis by ATLAS, will be an excellent probe. Thus, we encourage the experiments to perform such an analysis. Interference effects between the signal $gg \to H/A \to t\bar{t}$ and the background $gg \to t\bar{t}$ are known to be large, see Refs. [135–140], and due to the heavy SUSY spectrum in our example can be parametrized as a function of the Higgs masses and $\tan\beta$ for M_A values in the decoupling limit ($M_A \gg M_Z$).

4.3 $M_{h,\mathrm{EFT}}^{125}(\tilde{\chi})$ scenario

The second benchmark scenario we propose is the $M_{h,\mathrm{EFT}}^{125}(\tilde{\chi})$ scenario. In contrast to the $M_{h,\mathrm{EFT}}^{125}$ scenario, this scenario features light neutralinos and charginos whose presence significantly alters the Higgs phenomenology. We choose for the Higgsino, bino and wino mass parameters

$$\mu = 180\,\mathrm{GeV}, \quad M_1 = 160\,\mathrm{GeV}, \quad M_2 = 180\,\mathrm{GeV}, \quad (4)$$

respectively, such that this scenario represents an extension of the $M_h^{125}(\tilde{\chi})$ scenario [20] to low $\tan\beta$ values. The other input parameters are fixed according to Eq. (2), and the SUSY scale is again adjusted at every parameter point in order to obtain a light Higgs mass of $M_h \simeq 125\,\mathrm{GeV}$.

In Fig. 4 we present the $M_{h,\mathrm{EFT}}^{125}(\tilde{\chi})$ scenario in the (M_A, $\tan\beta$) parameter plane. The *green contour lines* show again the M_{SUSY} values required to reach $M_h \simeq 125\,\mathrm{GeV}$. The presence of light electroweakinos leads to an upwards shift of the SM-like Higgs-boson mass of ~ 1.5 GeV, therefore, smaller M_{SUSY} values are required as compared to the previous scenario. Again, we encounter a parameter region (*gray area*) at very low $M_A \lesssim 200$ GeV, for which M_{SUSY} would have to be chosen above 10^{16} GeV to obtain $M_h \geq 122$ GeV. However, in comparison to the $M_{h,\mathrm{EFT}}^{125}$ scenario, this region is slightly smaller due to the aforementioned contribution of the light electroweakinos to the light Higgs-boson mass.

We again show in Fig. 4 the direct constraints from LHC searches for non-SM-like Higgs bosons (*dashed black line* and *blue area*, with the *dark blue band* indicating the theoretical uncertainty) and indirect constraints from SM-like Higgs-boson signal-rate measurements (*dotted black line* and *hatched area*). The excluded area arising from direct searches for non-SM-like Higgs bosons – the relevant search channels are the same as in the $M_{h,\mathrm{EFT}}^{125}$ scenario (see above) – is smaller than in the previous case. In particular, $pp \to H/A \to \tau^+\tau^-$ searches only exclude M_A values up to 220 (400) GeV
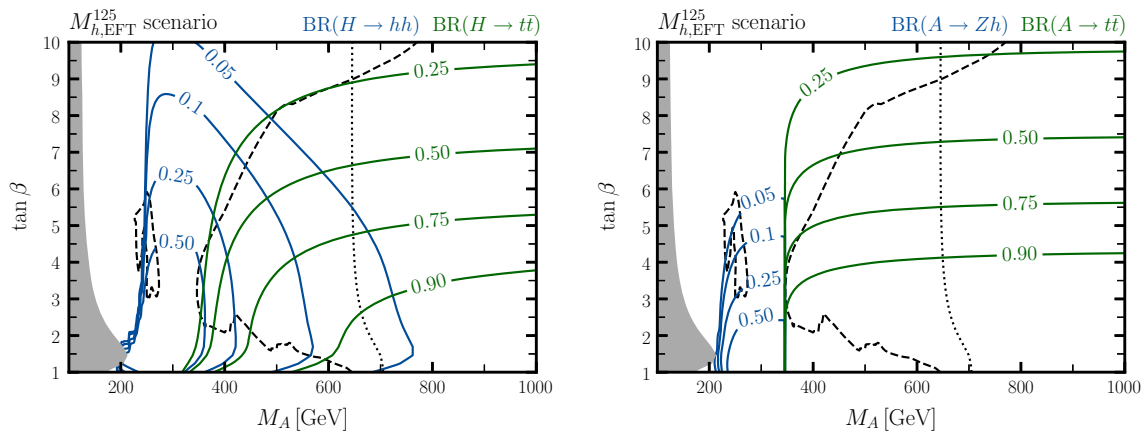
Fig. 3 *Left*: Branching ratios of the heavy $\mathcal{CP}$-even Higgs boson H into a pair of the light $\mathcal{CP}$-even Higgs bosons h (*blue*) and into a pair of top quarks (*green*) as a function of M_A and $\tan\beta$ in the $M_{h,\mathrm{EFT}}^{125}(\tilde{\chi})$ scenario. *Right*: Branching ratios of the $\mathcal{CP}$-odd Higgs boson A into a

Z-boson and the light $\mathcal{CP}$-even Higgs boson h (*blue*) and into a pair of top quarks (*green*). In each plot, the gray exclusion region and the boundaries of the blue and the hatched exclusion regions (shown as *dashed* and *dotted black lines*, respectively) of Fig. 1 are also depicted
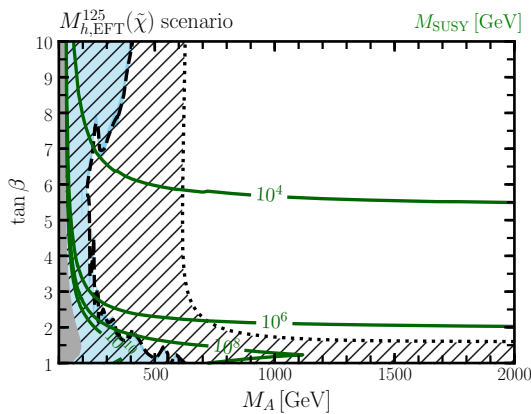
Fig. 4 The $M_{h,\mathrm{EFT}}^{125}(\tilde{\chi})$ benchmark scenario shown in the (M_A, $\tan\beta$) plane. The *green solid contour lines* show the required SUSY scale. The *black dotted line* and *hatched area* depict the 2σ disfavored region arising from the Higgs boson signal rate measurements. The *blue region* with the *black dashed boundary* is excluded at the 95% C.L by LHC searches for additional Higgs bosons (the *dark blue band* shows how the theoretical rate uncertainty affects the exclusion). The *gray area* is excluded because the mass of the SM-like Higgs boson h is below 122 GeV

Fig. 5 Contour lines of $M_h \simeq 125$ GeV (*solid*) and $M_h \simeq$ 122, 128 GeV (*dashed*) as a function of M_{SUSY} and $X_t^{\overline{\mathrm{DR}}}/M_{\mathrm{SUSY}}$), for $\tan\beta = 1$ (*blue*), $\tan\beta = 2.5$ (*red*) and $\tan\beta = 10$ (*green*). M_A is fixed to 1 TeV. All remaining parameters are as in the $M_{h,\mathrm{EFT}}^{125}(\tilde{\chi})$ scenario. The *orange star* marks the approximate position of the $M_h^{125}(\tilde{\chi})$ scenario [20]

for moderately large $\tan\beta$ values of 6 (10). For $\tan\beta$ values between 2 and 6 the parameter space for $M_A \lesssim 250$ GeV is constrained mostly by $pp \rightarrow H \rightarrow ZZ$ searches. The low $\tan\beta$ region is again constrained by $pp \rightarrow H \rightarrow hh$ searches and charged Higgs-boson searches. The decrease in sensitivity of all these search channels with respect to the previous scenario arises from the fact that the heavy Higgs bosons H and A can decay to pairs of light electroweakinos. If such decays have sizable rates, the branching ratios for heavy Higgs-boson decays to SM particles are suppressed. We will discuss the heavy Higgs-boson decays to electroweakinos in detail below.
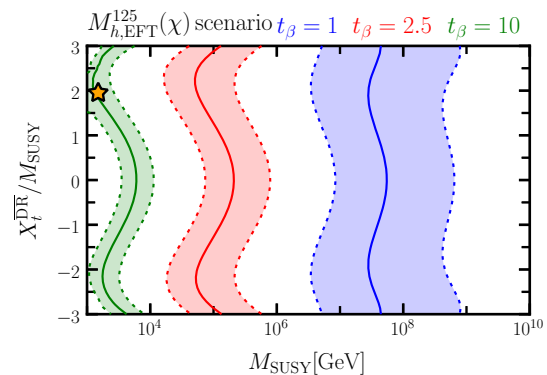
In Fig. 4 the parameter region at $M_A \lesssim 630$ GeV is excluded by the SM-like Higgs-boson signal-strength measurements. In comparison to the $M_{h,\mathrm{EFT}}^{125}$ scenario, however, an additional exclusion arises in the region of very small $\tan\beta$ values $\lesssim 1.5$ (depending on M_A). In this area the branching ratio of the light Higgs decay to two photons, $h \rightarrow \gamma\gamma$, is significantly enhanced due to the presence of light charginos. We will also explore this decay mode below.

Figure 5 shows the $M_h = 125$ GeV contours (*solid*) around the $M_{h,\mathrm{EFT}}^{125}(\tilde{\chi})$ scenario as a function of M_{SUSY} and $X_t^{\overline{\mathrm{DR}}}/M_{\mathrm{SUSY}}$ for $\tan\beta = 1$ (*blue*), $\tan\beta = 2.5$ (*red*) and $\tan\beta = 10$ (*green*). In comparison to the previous benchmark scenario, see Fig. 2, the Higgs-boson mass contours are shifted by approximately half an order of magnitude to

lower M_{SUSY} values. As mentioned before, this shift originates from the presence of light electroweakinos in this scenario which lead to an upwards shift of the light Higgs-boson mass. For comparison, we also show the approximate position of the $M_h^{125}(\tilde{\chi})$ scenario of Ref. [20], for which $M_{SUSY} = 1.5$ TeV and $X_t^{OS} = 2.5$ TeV. Keep in mind the different renormalization schemes: Ref. [20] employs X_t^{OS}, whereas this work is based on $X_t^{\overline{DR}}$.

We now discuss in detail the impact of the light electroweakinos on the decays of the MSSM Higgs bosons. Such decays were already considered in early discussions of discovery prospects of the CMS detector [141–143] and were advocated by theorists in recent years [46,144–152], see e.g. Ref. [153] for a thorough analysis on the sensitivity in a class of benchmark scenarios. The electroweakino spectrum is fixed at tree-level by the choice of μ, M_1, M_2 and the value of $\tan\beta$ and exhibits a strong wino-Higgsino mixing in both the neutralino and chargino sector. This mixing, which pushes the wino and Higgsino mass eigenstates away from each other, is enhanced for small values of $\tan\beta$, such that at $\tan\beta = 1$ the spectrum is slightly less compressed than at $\tan\beta = 10$. The lightest neutralino mass increases from ~ 85 GeV to ~ 112 GeV between $\tan\beta = 1$ and $\tan\beta = 10$. In the *left panel* of Fig. 6 we show the partial width of the decay $h \to \gamma\gamma$ normalized to the SM prediction. The decay width is enhanced by $\gtrsim 20\%$ for low $\tan\beta \lesssim 2$. This enhancement originates from loop corrections involving light charginos. As discussed above, our choice of $M_2 = \mu$ in this scenario leads to a significant wino-Higgsino mixing in the chargino sector, which, in turn, results in a large coupling of the charginos to the MSSM Higgs bosons. Hence, we have a sizable contribution to $h \to \gamma\gamma$ from charginos in this scenario. The distortions for $M_A \lesssim 200$ GeV are due

to sizable mixing effects between the h and H bosons. In the *right panel* of Fig. 6 we show the branching ratio of the decay $h \to \gamma\gamma$ normalized to its SM prediction. In comparison to the partial width, the enhancement of the $h \to b\bar{b}$ decay width in the low-M_A regime leads to an additional suppression of the branching ratio of the $h \to \gamma\gamma$ decay. For large M_A values above around 800 GeV and $\tan\beta \lesssim 2$, the branching ratio is enhanced by $\gtrsim 15\%$, which yields the exclusion from the $h \to \gamma\gamma$ signal rate measurement at very low $\tan\beta$ values, which persists in the Higgs decoupling regime ($M_A \gg M_Z$). Future precision measurements of this Higgs-boson decay mode thus offer the possibility to indirectly probe for light electroweakinos within this scenario, even if the remaining Higgs bosons are very heavy. On the other hand, if the branching ratio $h \to \gamma\gamma$ remains to be consistent with the SM predictions in the future, the lower bound on $\tan\beta$ will be increased. This will in turn lead to a more stringent upper bound on the SUSY scale (see Fig. 5).

Figure 7 shows the branching ratios for the decays of the heavy Higgs bosons H (*left panel*) and A (*right panel*) into pairs of charginos and neutralinos. The contributions from all kinematically accessible electroweakino final states are summed. For both H and A the branching ratio into electroweakinos exceeds 80% for $\tan\beta \gtrsim 4$ and $M_A \gtrsim 500$ GeV. When decreasing M_A below 500 GeV, we encounter kinematic thresholds where some decay modes into electroweakinos become inaccessible, leading to a gradual decrease with sharp transitions of the inclusive Higgs-to-electroweakino branching ratio. The structures at $M_A \sim 340$ GeV are caused by the kinematic threshold for the decays into a pair of top quarks. The large branching ratios for the decays into electroweakinos strongly motivates dedicated LHC searches for
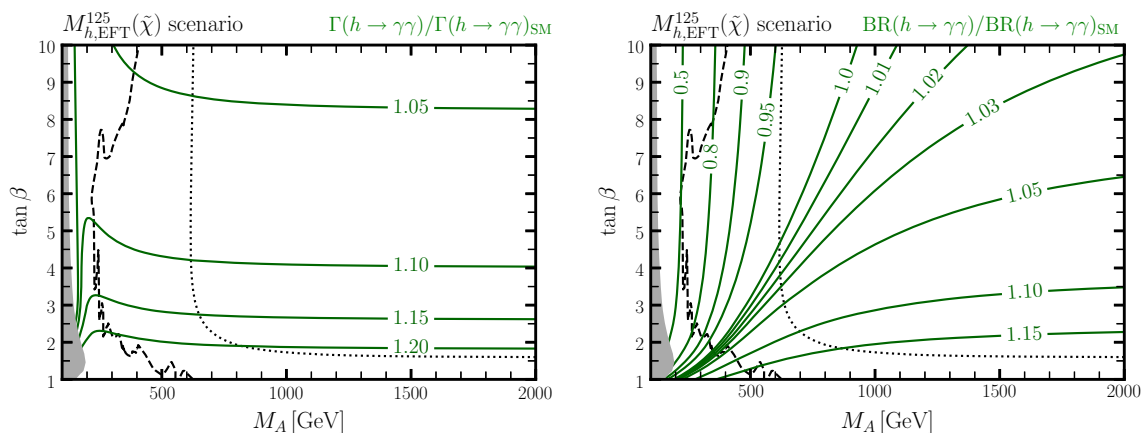

Fig. 6 *Left*: Decay width of the light $\mathcal{CP}$-even Higgs boson h into photons (*green contour lines*) in the (M_A, $\tan\beta$) plane in the $M_{h,EFT}^{125}(\tilde{\chi})$ scenario, normalized to the corresponding SM prediction. *Right*: Branching ratio of the decay $h \to \gamma\gamma$, normalized to its SM prediction (*green contour lines*). In each plot, the gray exclusion region and the boundaries of the blue and the hatched exclusion regions (shown as *dashed* and *dotted black lines*, respectively) of Fig. 4 are also depicted
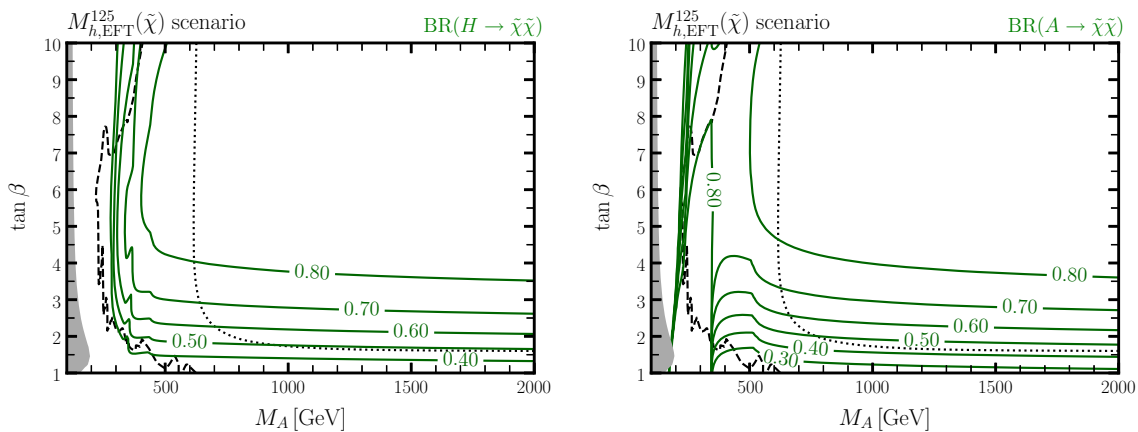
Fig. 7 Branching ratios of the decays of the heavy $\mathcal{CP}$-even Higgs boson H (*left*) and the $\mathcal{CP}$-odd Higgs boson A (*right*) into electroweakino pairs, shown in the $(M_A, \tan\beta)$ plane in the $M_{h,\mathrm{EFT}}^{125}(\tilde{\chi})$ scenario. The contributions from all kinematically allowed combina-

tions of electroweakinos in the final state are summed. In each plot, the gray exclusion region and the boundaries of the blue and the hatched exclusion regions (shown as *dashed* and *dotted black lines*, respectively) of Fig. 4 are also depicted

these signatures. We will discuss the most promising signatures in detail below.

The presence of light electroweakinos also affects the decay rates of the charged Higgs boson $H^{\pm}$. In the *right panel* of Fig. 8 we show the branching ratio of the charged Higgs boson decaying into neutralino-chargino pairs. Again, the contributions from all kinematically accessible electroweakino final states are summed. Similar as for the neutral Higgs bosons, the branching ratio for charged Higgs-boson decays to electroweakinos exceeds 80% for large $M_A \gtrsim 700\,\mathrm{GeV}$ and $\tan\beta \gtrsim 4$. We furthermore provide in the *left panel* of Fig. 8 the production cross section (in fb) for top-quark associated production of a negatively charged Higgs boson (the charge-conjugated process has identical production rate) at the LHC with a center-of-mass energy of 13 TeV. While most of the parameter region with large cross section is already strongly constrained by the SM-like Higgs-boson signal-rate measurements, the production cross section can still exceed 10 fb in the allowed parameter space at $\tan\beta \sim 3$ and $M_A \sim 700\,\mathrm{GeV}$. Together with a decay rate to electroweakinos of $60 - 70\%$, the signal cross section for $pp \to tH^{\pm} \to t(\chi^{\pm}\chi)$ can still be $\gtrsim 14$ fb, corresponding to more than 2200 expected signal events in the currently recorded integrated luminosity of LHC Run-2 per experiment, $\mathcal{L}_{\mathrm{int}} \simeq 160\ \mathrm{fb}^{-1}$. Thus, searches for a charged Higgs boson decaying into electroweakinos could be a promising way to further probe the $M_{h,\mathrm{EFT}}^{125}(\tilde{\chi})$ scenario.

To disentangle in detail the different decay channels of the heavy Higgs bosons, Fig. 9 shows the branching ratios for the dominant decay modes of the $\mathcal{CP}$-even heavy Higgs boson H into SM particles (including the light Higgs boson h) (*left panels*) and SUSY particles (*right panels*) as a function of M_A, focusing on the region $200\,\mathrm{GeV} \le M_A \le 1000\,\mathrm{GeV}$,

for $\tan\beta = 2.5$ (*upper panels*) and $\tan\beta = 7.5$ (*lower panels*). For $\tan\beta = 2.5$ the decays into SM particles dominate for $M_A \lesssim 350\,\mathrm{GeV}$ with the strongest decays modes being $H \to W^{\pm}W^{\mp}, ZZ$ (for $M_A \lesssim 250\,\mathrm{GeV}$) and $H \to hh$ (for $M_A \gtrsim 250\,\mathrm{GeV}$). In the M_A range between $280\,\mathrm{GeV}$ and $360\,\mathrm{GeV}$, the dominant H decay to electroweakinos is $H \to \tilde{\chi}_1\tilde{\chi}_3$, featuring a decay rate of up to 30%. For $M_A \gtrsim 350\,\mathrm{GeV}$, the decay into a pair of top quarks becomes kinematically accessible, reaching around 30% at high M_A values, and leading to a suppression of the other decay modes. In this M_A range, all other relevant decays contain electroweakinos in the final state, with the dominant decay modes being $H \to \tilde{\chi}_1^{\pm}\tilde{\chi}_2^{\mp}$ ($\sim 30\%$), $H \to \tilde{\chi}_1\tilde{\chi}_3$ ($\sim 10\%$) and $H \to \tilde{\chi}_3\tilde{\chi}_4$ ($\sim 10\%$).

For $\tan\beta = 7.5$, the H decay into a top-quark pair is suppressed, while the decay into a bottom-quark pair and a τ-lepton pair is enhanced. In particular, the latter decays play a significant role for $M_A \lesssim 380\,\mathrm{GeV}$, whereas the H decays to vector bosons or light Higgs bosons are negligible. In this low M_A range, the dominant Higgs-to-electroweakino decays are to the lighter states, $H \to \tilde{\chi}_1^{\pm}\tilde{\chi}_1^{\mp}$, the invisible decay $H \to \tilde{\chi}_1\tilde{\chi}_1$ and $H \to \tilde{\chi}_1\tilde{\chi}_3$, reaching decay rates of around 30%, 20% and 17%, respectively, at $M_A \simeq 380\,\mathrm{GeV}$. At larger M_A values, the H decays are strongly dominated by the electroweakino final states, with $H \to \tilde{\chi}_1^{\pm}\tilde{\chi}_2^{\mp}$ ($\sim 30\%$), $H \to \tilde{\chi}_1^{\pm}\tilde{\chi}_1^{\mp}$ ($\sim 20\%$), $H \to \tilde{\chi}_1\tilde{\chi}_4$ ($\sim 12\%$) and $H \to \tilde{\chi}_1\tilde{\chi}_1$ ($\sim 10\%$) being the dominant decay modes. In general, for both $\tan\beta$ values, we observe that the branching ratios are almost constant for $M_A \gtrsim 500\,\mathrm{GeV}$, i.e. as soon as all decays of H into pairs of electroweakinos are kinematically open.

We now turn to the decays of the $\mathcal{CP}$-odd Higgs boson A in the $M_{h,\mathrm{EFT}}^{125}(\tilde{\chi})$ scenario, which are shown in Fig. 10 in anal-
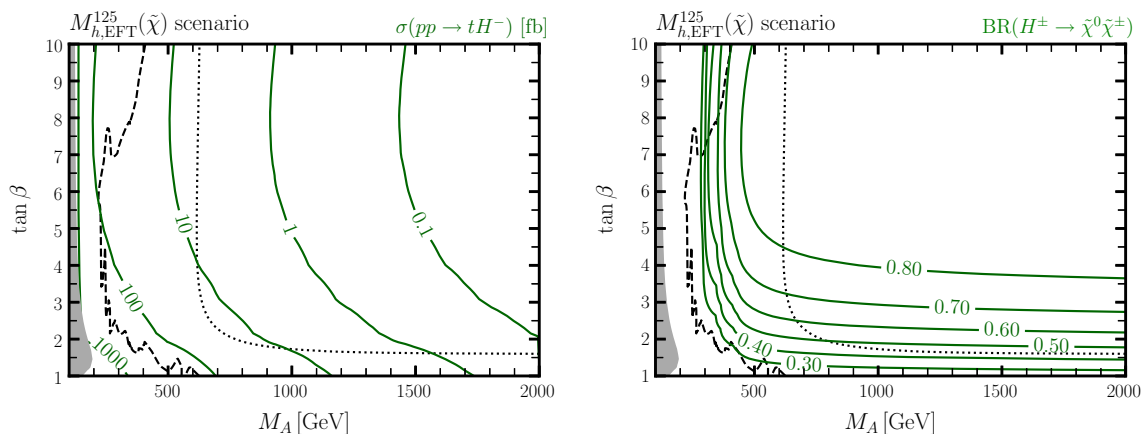
Fig. 8 Charged Higgs-boson phenomenology in the $M_{h,\text{EFT}}^{125}(\tilde{\chi})$ scenario. *Left*: Production cross section (in fb) of a negatively charged Higgs boson H^- in association with a top quark (*green contour lines*) at the LHC with 13 TeV center-of-mass energy. *Right*: Branching ratio of the charged Higgs boson decaying into chargino–neutralino pairs

(*green contour lines*). The contributions from all kinematically allowed combinations of electroweakinos in the final state are summed. In each plot, the gray exclusion region and the boundaries of the blue and the hatched exclusion regions (shown as *dashed* and *dotted black lines*, respectively) of Fig. 4 are also depicted
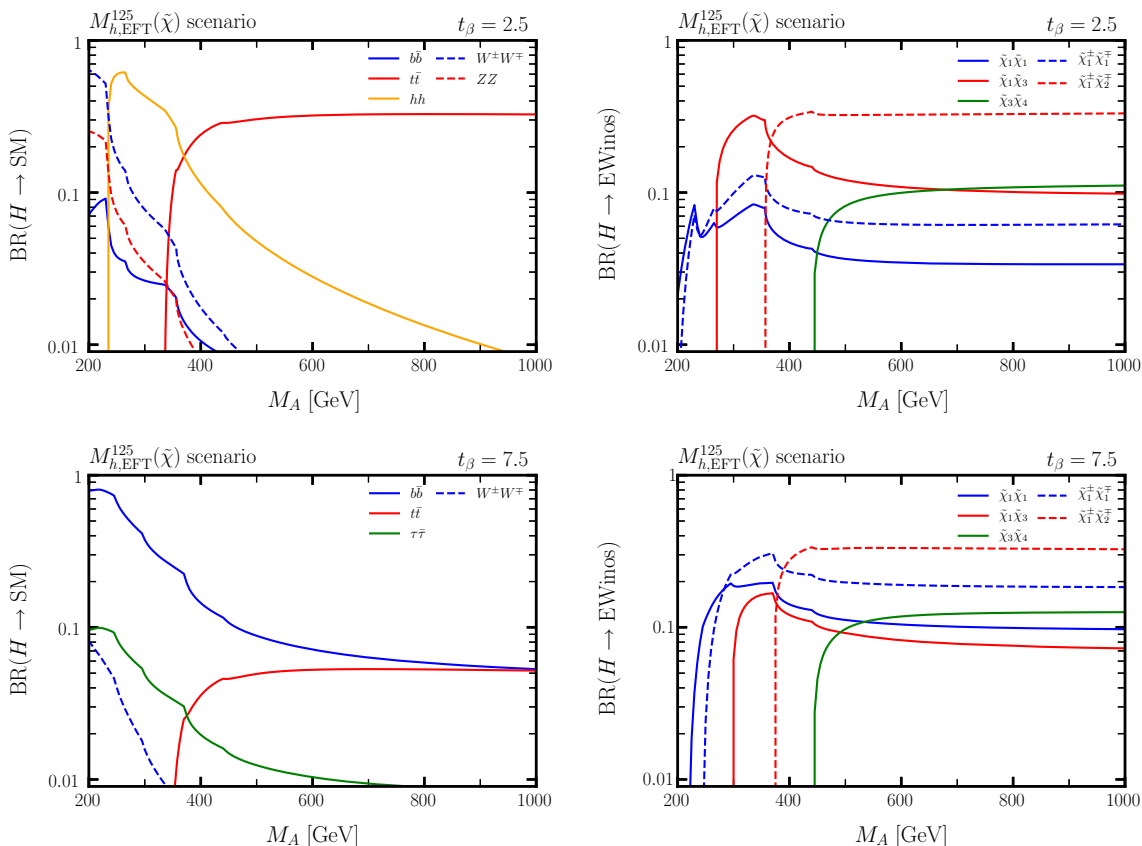
Fig. 9 Branching ratios for the decays of the heavy $\mathcal{CP}$-even Higgs boson H in the $M_{h,\text{EFT}}^{125}(\tilde{\chi})$ scenario as a function of M_A, for fixed $\tan\beta = 2.5$ (*upper panels*) and 7.5 (*lower panels*). The dominant decays into SM particles (*left panels*) and electroweakinos (*right panels*) are displayed
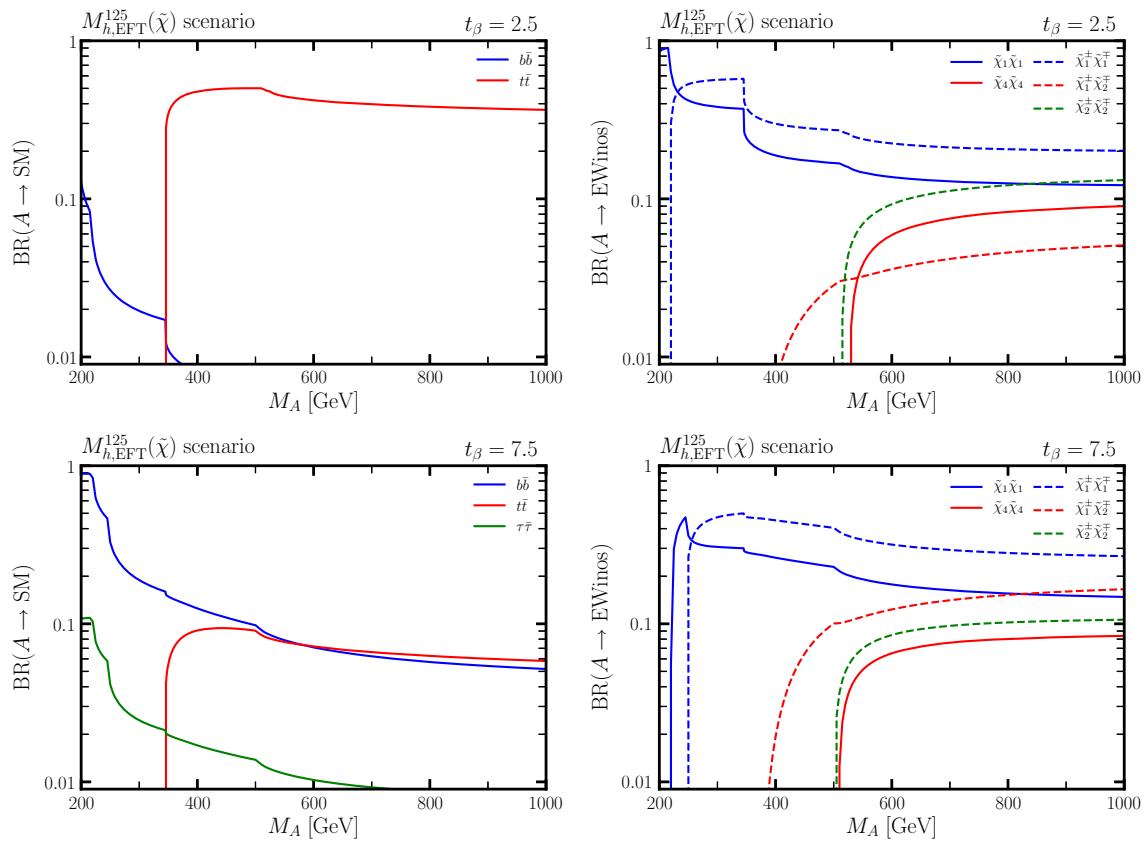
Fig. 10 Branching ratios for the decays of the $\mathcal{CP}$-odd Higgs boson A in the $M_{h,\mathrm{EFT}}^{125}(\tilde{\chi})$ scenario as a function of M_A, for fixed $\tan\beta = 2.5$ (*upper panels*) and 7.5 (*lower panels*). The dominant decays into SM particles (*left panels*) and electroweakinos (*right panels*) are displayed

ogy to Fig. 9. For $\tan\beta = 2.5$, the decays into SM particles only play a minor role below the threshold for decays into a top-quark pair. In this region, the Higgs-to-electroweakino decays $A \to \tilde{\chi}_1\tilde{\chi}_1$ and $A \to \tilde{\chi}_1^{\pm}\tilde{\chi}_1^{\mp}$ are dominant. Above the top-quark pair threshold, the A boson dominantly decays into $t\bar{t}$ with branching ratios of $\sim 40\%$ to 50% and the decay modes into electroweakino pairs $A \to \tilde{\chi}_1^{\pm}\tilde{\chi}_1^{\mp}$ and $A \to \tilde{\chi}_1\tilde{\chi}_1$ drop to $\sim 20\%$ and $\sim 12\%$, respectively. Other electroweakino final states become accessible at higher M_A values, however, they remain mostly subdominant.

For $\tan\beta = 7.5$, the pattern of A decays to SM particles changes significantly. Below the $A \to t\bar{t}$ kinematic threshold, the decay $A \to b\bar{b}$ dominates. Once the electroweakino final states become kinematically accessible for $M_A \gtrsim 220\,\mathrm{GeV}$, the invisible decay $A \to \tilde{\chi}_1\tilde{\chi}_1$ and the decay $A \to \tilde{\chi}_1^{\pm}\tilde{\chi}_1^{\mp}$ reach values of up to $40-50\%$, thus leading to a strong suppression of A decays to SM final states. Once the decay $A \to \tilde{\chi}_1^{\pm}\tilde{\chi}_1^{\mp}$ is open, it remains the dominant decay mode with a rate of $\sim 30\%$ at high M_A values. Here, the next-to-highest decays rates are obtained for $A \to \tilde{\chi}_1^{\pm}\tilde{\chi}_2^{\mp}$ and $A \to \tilde{\chi}_1\tilde{\chi}_1$, amounting to around $10-20\%$ each. The decays to SM particles, i.e. $A \to t\bar{t}$ and $A \to b\bar{b}$, have a combined branching ratio of $\sim 11\%$ at large M_A.

Lastly, we study in detail the decays of the charged Higgs boson in Fig. 11 in analogy to Figs. 9 and 10. For $\tan\beta = 2.5$, the dominant decay mode is $H^+ \to t\bar{b}$, which does not fall below 35% in the considered M_A range. The decays into neutralino-chargino pairs, once they become kinematically accessible, are all comparable in size, with the strongest modes reaching branching ratios of $\sim 12\%$. For $\tan\beta = 7.5$, the overall behavior of the various decay modes is very similar to the case of $\tan\beta = 2.5$. For $M_A \lesssim 300\,\mathrm{GeV}$, however, the branching ratio into $t\bar{b}$ is reduced by $\sim 20-30\%$, while the decay to $\tau^+\nu_\tau$ is much more important, with decay rates of up to 30%. Also the branching ratios for decays into neutralino-chargino pairs is increased, with $\mathrm{BR}(H^+ \to \tilde{\chi}_2\tilde{\chi}_1^{\pm})$ reaching values up to 30% for $M_A \sim (280-360)\,\mathrm{GeV}$. The fact that the rates of various H^+-to-electroweakino decays are very similar warrants a combined experimental search for the various signatures arising from these decays within this benchmark model.

The previous figures clearly show that decay rates of heavy neutral and charged Higgs bosons to electroweakinos can be sizable in the $M_{h,\mathrm{EFT}}^{125}(\tilde{\chi})$ scenario. This strongly motivates dedicated searches for these type of decays. In the remaining part of this section we will therefore discuss such decays
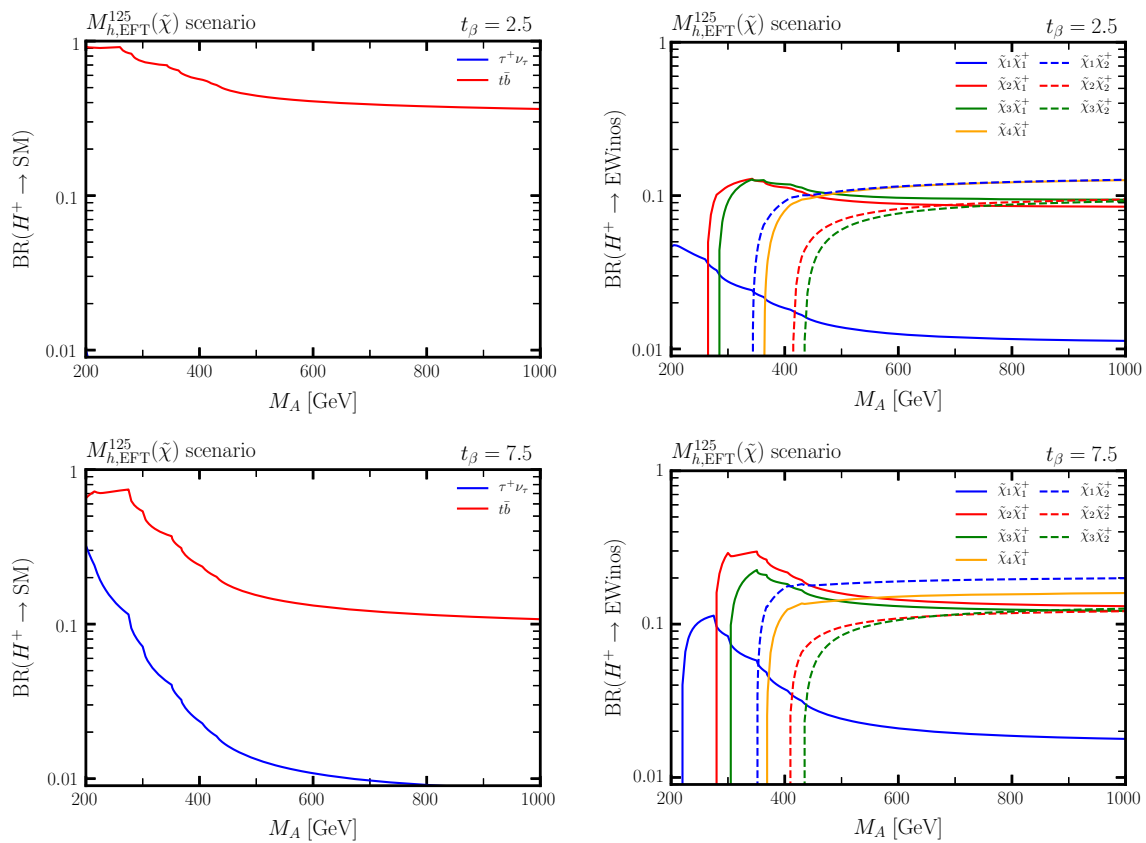
Fig. 11 Branching ratios for the decays of the charged Higgs boson H^+ in the $M_{h,\mathrm{EFT}}^{125}(\tilde{\chi})$ scenario as a function of M_A, for fixed $\tan\beta = 2.5$ (*upper panels*) and 7.5 (*lower panels*). The dominant decays into SM particles (*left panels*) and electroweakinos (*right panels*) are displayed

in more detail, focusing on a few representative parameter points.

Typically, LHC searches for electroweakino pairs that are produced via the conventional processes, namely s-channel vector-boson exchange and t-channel squark exchange, and decay to the lightest supersymmetric particle (LSP) – the lightest neutralino, $\tilde{\chi}_1$ – by emitting a W- or a Z-boson, select events with ≥ 2 leptons (i.e., electrons and muons) and large missing transverse energy, $\not{E}_T$, see e.g. Refs. [154–159] for recent LHC searches. However, their sensitivity is significantly deteriorated when the mass difference between the decaying electroweakino and the LSP is small. In this case, the emitted off-shell vector boson can only yield a low-p_T ("soft") lepton that often does not pass the lepton-reconstruction criteria. Dedicated searches for such compressed electroweakino mass spectra have been designed [160,161], which require additional jet(s) from initial-state radiation (ISR) against which the produced electroweakinos recoil, thus giving an additional boost to the final-state leptons. However, these searches pay the price of a lower expected signal-event yield due to the ISR jet(s) requirement, and can therefore only cover the parameter space with very light electroweakinos.

The $M_{h,\mathrm{EFT}}^{125}(\tilde{\chi})$ scenario features a heavily-mixed electroweakino sector, such that the limits obtained by the direct LHC searches mentioned above cannot be directly applied. These are obtained under certain simplifying assumptions, e.g., for the stronger, "pure wino" production scenario of Refs. [160,161]: (1) the produced neutralinos and charginos are pure winos, (2) their masses are equal, and (3) they decay to 100% into the lightest neutralino and a Z- or a W-boson, respectively. If these assumptions are fulfilled, current results with $36\,\mathrm{fb}^{-1}$ of 13 TeV data exclude "wino" masses of around $180 - 230\,\mathrm{GeV}$ for mass differences to the LSP between $5\,\mathrm{GeV}$ and $25\,\mathrm{GeV}$. We expect these searches to also exhibit some sensitivity to the electroweakino spectrum of the $M_{h,\mathrm{EFT}}^{125}(\tilde{\chi})$ scenario, however, it is unclear whether they indeed exclude this scenario, given the complexity of its mass and decay spectrum (see below for details). We therefore strongly encourage dedicated analyses optimized for our and similar scenarios by the experiments.

In Table 1 we provide detailed information on the masses and dominant production and decay modes of the neutralinos and charginos in the $M_{h,\mathrm{EFT}}^{125}(\tilde{\chi})$ benchmark scenario, for $\tan\beta$ values of 2.5 (scenario 1) and 7.5 (scenario 2). We calculated the direct neutralino/chargino production cross sec-

Table 1 A detailed view on two parameter points from the $M_{h,\mathrm{EFT}}^{125}(\tilde{\chi})$ scenario (scenario 1 and 2), as well as two variations (scenario 3 and 4): relevant parameters for the electroweak sector (top); masses and rates for the dominant production modes (for the LHC at 13 TeV) and decay modes of the neutralinos and charginos (bottom)

	Scenario 1	Scenario 2	Scenario 3	Scenario 4
μ (GeV)	180	180	280	280
M_1 (GeV)	160	160	260	260
M_2 (GeV)	180	180	280	280
$\tan\beta$	2.5	7.5	2.5	7.5
Neutralino and chargino masses, production and decay rates				
$m_{\tilde{\chi}_1}$ (GeV)	95.8	110.0	194.8	207.9
$m_{\tilde{\chi}_2}$ (GeV)	164.6	164.7	264.6	254.7
$m_{\tilde{\chi}_3}$ (GeV)	183.8	188.8	282.4	285.6
$m_{\tilde{\chi}_4}$ (GeV)	263.4	254.1	362.9	353.0
$m_{\tilde{\chi}_1^\pm}$ (GeV)	108.9	122.7	207.9	220.4
$m_{\tilde{\chi}_2^\pm}$ (GeV)	256.6	250.3	355.7	348.1
$\sigma(pp \to \tilde{\chi}_1\tilde{\chi}_3)$ (fb)	407.0	329.0	58.7	52.3
$\sigma(pp \to \tilde{\chi}_3\tilde{\chi}_4)$ (fb)	77.1	77.1	18.8	19.2
$\sigma(pp \to \tilde{\chi}_1^\pm\tilde{\chi}_1)$ (fb)	8661.0	5206.0	754.0	579.4
$\sigma(pp \to \tilde{\chi}_1^\pm\tilde{\chi}_2)$ (fb)	974.0	866.0	135.0	128.3
$\sigma(pp \to \tilde{\chi}_1^\pm\tilde{\chi}_3)$ (fb)	660.0	547.0	102.0	91.9
$\sigma(pp \to \tilde{\chi}_1^\pm\tilde{\chi}_4)$ (fb)	87.7	99.0	18.7	20.0
$\sigma(pp \to \tilde{\chi}_2^\pm\tilde{\chi}_2)$ (fb)	132.0	136.0	31.0	31.5
$\sigma(pp \to \tilde{\chi}_2^\pm\tilde{\chi}_3)$ (fb)	154.0	160.0	37.3	38.7
$\sigma(pp \to \tilde{\chi}_2^\pm\tilde{\chi}_4)$ (fb)	331.2	371.0	92.9	102.3
$\sigma(pp \to \tilde{\chi}_1^\pm\tilde{\chi}_1^\mp)$ (fb)	4613.0	2999.7	440.0	352.2
$\sigma(pp \to \tilde{\chi}_1^\pm\tilde{\chi}_2^\mp)$ (fb)	71.4	65.6	15.2	14.3
$\sigma(pp \to \tilde{\chi}_2^\pm\tilde{\chi}_2^\mp)$ (fb)	199.0	217.2	54.5	58.9
BR$(\tilde{\chi}_2 \to \ldots)$	100.0% $(\tilde{\chi}_1^\pm W^{\mp *})$	99.0% $(\tilde{\chi}_1^\pm W^{\mp *})$	100% $(\tilde{\chi}_1^\pm W^{\mp *})$	100% $(\tilde{\chi}_1^\pm W^{\mp *})$
BR$(\tilde{\chi}_3 \to \ldots)$	54.8% $(\tilde{\chi}_1^\pm W^{\mp *})$	55.5% $(\tilde{\chi}_1^\pm W^{\mp *})$	52.2% $(\tilde{\chi}_1^\pm W^{\mp *})$	52.4% $(\tilde{\chi}_1^\pm W^{\mp *})$
	45.2% $(\tilde{\chi}_1^0 Z^*)$	44.5% $(\tilde{\chi}_1^0 Z^*)$	47.8% $(\tilde{\chi}_1^0 Z^*)$	47.6% $(\tilde{\chi}_1^0 Z^*)$
BR$(\tilde{\chi}_4^0 \to \ldots)$	99.5% $(\tilde{\chi}_1^\pm W^\mp)$	99.1% $(\tilde{\chi}_1^\pm W^\mp)$	99.8% $(\tilde{\chi}_1^\pm W^\mp)$	99.5% $(\tilde{\chi}_1^\pm W^\mp)$
BR$(\tilde{\chi}_1^\pm \to \ldots)$	100% $(\tilde{\chi}_1^0 W^{\pm *})$	100% $(\tilde{\chi}_1^0 W^{\pm *})$	100% $(\tilde{\chi}_1^0 W^{\pm *})$	100% $(\tilde{\chi}_1^0 W^{\pm *})$
BR$(\tilde{\chi}_2^\pm \to \ldots)$	53.4% $(\tilde{\chi}_1^\pm Z)$	51.5% $(\tilde{\chi}_1^\pm Z)$	53.7% $(\tilde{\chi}_1^\pm Z)$	52.7% $(\tilde{\chi}_1^\pm Z)$
	38.0% $(\tilde{\chi}_1^0 W^\pm)$	41.8% $(\tilde{\chi}_1^0 W^\pm)$	40.1% $(\tilde{\chi}_1^0 W^\pm)$	44.7% $(\tilde{\chi}_1^0 W^\pm)$

tions for the LHC at a center-of-mass energy of 13 TeV at the NLO+NLL level using `Resummino` (version 2.0.1) [162–166] with the CT14 PDF sets [167]. The value of M_A does not affect the electroweakino spectrum at tree-level, however, it obviously affects the heavy Higgs-boson phenomenology. In Table 2 we provide for these scenarios the 13 TeV cross sections for the dominant heavy Higgs-boson production modes, as well as the rates for the three dominant decays to electroweakinos, for $M_A = 1$ TeV.

For the heavy $\mathcal{CP}$-even Higgs boson H we identify the cascade decay

$$H \to \tilde{\chi}_1^\pm\tilde{\chi}_2^\mp \to (\tilde{\chi}_1 W^{\pm *})(\tilde{\chi}_1^\mp Z) \to \tilde{\chi}_1\tilde{\chi}_1 W^{\pm *}W^{\mp *}Z$$
(5)

as the most frequent process, with a total rate of around 17.7% (16.8%) for $\tan\beta = 2.5$ (7.5). Despite their off-shellness, one can still expect reasonably high-p_T leptons from the W-bosons, provided that $M_H \gg (m_{\tilde{\chi}_1^\pm} + m_{\tilde{\chi}_2^\pm})$, as is the case in this example. This process can therefore lead to a spectacular signature with up to 4 reconstructable leptons, missing transverse energy, and for larger $\tan\beta$ values possibly two additional b-jets, if the heavy Higgs boson is produced in association with bottom quarks. Moreover, many of the other possible cascade decays also lead to final states with multiple W- and or Z-bosons. In contrast, the direct (invisible) Higgs-boson decay into two lightest neutralinos, $H \to \tilde{\chi}_1\tilde{\chi}_1$, as well as decays leading to a $Z + \not{E}_T$ final state (e.g., via $H \to \tilde{\chi}_1\tilde{\chi}_3 \to \tilde{\chi}_1\tilde{\chi}_1 Z$) occur with smaller rates,

Table 2 A detailed view on two parameter points from the $M_{h,\mathrm{EFT}}^{125}(\tilde{\chi})$ scenario (scenario 1 and 2), as well as two variations (scenario 3 and 4): relevant parameters for the electroweak sector (top); rates of the dominant production modes (for the LHC at 13 TeV) and decay modes to electroweakinos of the heavy Higgs bosons H, A and H^+, for fixed $M_A = 1$ TeV (bottom)

	Scenario 1	Scenario 2	Scenario 3	Scenario 4
μ (GeV)	180	180	280	280
M_1 (GeV)	160	160	260	260
M_2 (GeV)	180	180	280	280
$\tan\beta$	2.5	7.5	2.5	7.5
MSSM Higgs boson production and decay rates for $M_A = 1$ TeV				
$\sigma(gg \to H)$ (fb)	19.0	1.8	19.0	1.8
$\sigma(b\bar{b} \to H)$ (fb)	0.6	5.1	0.6	5.1
$\sigma(gg \to A)$ (fb)	24.6	3.6	24.6	3.6
$\sigma(b\bar{b} \to A)$ (fb)	0.6	5.1	0.6	5.1
$\sigma(pp \to tH^-)$ (fb)	3.7	0.7	3.7	0.7
BR($H \to \tilde{\chi}\tilde{\chi}$)	33.1% ($\tilde{\chi}_1^\pm \tilde{\chi}_2^\mp$)	32.6% ($\tilde{\chi}_1^\pm \tilde{\chi}_2^\mp$)	33.0% ($\tilde{\chi}_1^\pm \tilde{\chi}_2^\mp$)	36.0% ($\tilde{\chi}_1^\pm \tilde{\chi}_2^\mp$)
	11.1% ($\tilde{\chi}_3 \tilde{\chi}_4$)	18.4% ($\tilde{\chi}_1^\pm \tilde{\chi}_1^\mp$)	10.9% ($\tilde{\chi}_1 \tilde{\chi}_3$)	14.4% ($\tilde{\chi}_1^\pm \tilde{\chi}_1^\mp$)
	9.8% ($\tilde{\chi}_1 \tilde{\chi}_3$)	12.6% ($\tilde{\chi}_3 \tilde{\chi}_4$)	10.4% ($\tilde{\chi}_3 \tilde{\chi}_4$)	12.4% ($\tilde{\chi}_3 \tilde{\chi}_4$)
BR($A \to \tilde{\chi}\tilde{\chi}$)	20.2% ($\tilde{\chi}_1^\pm \tilde{\chi}_1^\mp$)	26.8% ($\tilde{\chi}_1^\pm \tilde{\chi}_1^\mp$)	19.6% ($\tilde{\chi}_1^\pm \tilde{\chi}_1^\mp$)	26.1% ($\tilde{\chi}_1^\pm \tilde{\chi}_1^\mp$)
	13.2% ($\tilde{\chi}_2^\pm \tilde{\chi}_2^\mp$)	16.6% ($\tilde{\chi}_1^\pm \tilde{\chi}_2^\mp$)	12.5% ($\tilde{\chi}_2^\pm \tilde{\chi}_2^\mp$)	14.0% ($\tilde{\chi}_1^\pm \tilde{\chi}_2^\mp$)
	12.2% ($\tilde{\chi}_1 \tilde{\chi}_1$)	14.8% ($\tilde{\chi}_1 \tilde{\chi}_1$)	12.2% ($\tilde{\chi}_1 \tilde{\chi}_1$)	15.2% ($\tilde{\chi}_1 \tilde{\chi}_1$)
BR($H^+ \to \tilde{\chi}\tilde{\chi}^+$)	12.7% ($\tilde{\chi}_1 \tilde{\chi}_2^+$)	19.9% ($\tilde{\chi}_1 \tilde{\chi}_2^+$)	12.3% ($\tilde{\chi}_4 \tilde{\chi}_1^+$)	17.4% ($\tilde{\chi}_1 \tilde{\chi}_2^+$)
	12.6% ($\tilde{\chi}_4 \tilde{\chi}_1^+$)	16.0% ($\tilde{\chi}_4 \tilde{\chi}_1^+$)	11.2% ($\tilde{\chi}_1 \tilde{\chi}_2^+$)	16.6% ($\tilde{\chi}_4 \tilde{\chi}_1^+$)
	9.4% ($\tilde{\chi}_2 \tilde{\chi}_2^+$)	13.1% ($\tilde{\chi}_2 \tilde{\chi}_1^+$)	9.5% ($\tilde{\chi}_3 \tilde{\chi}_1^+$)	13.1% ($\tilde{\chi}_3 \tilde{\chi}_1^+$)
BR($h \to \gamma\gamma$)$_{\mathrm{MSSM/SM}}$	1.12	1.02	1.02	0.98

e.g. with branching ratios of 3.4% and 4.4%, respectively, in scenario 1.[12]

For the $\mathcal{CP}$-odd Higgs boson A, the most frequent process is

$$A \to \tilde{\chi}_1^\pm \tilde{\chi}_1^\mp \to \tilde{\chi}_1 \tilde{\chi}_1 W^{\pm *} W^{\mp *} \tag{6}$$

with a rate of 20.2% (26.5%) for $\tan\beta = 2.5$ (7.5). Experimentally more promising, however, might be the cascade

$$A \to \tilde{\chi}_2^\pm \tilde{\chi}_2^\mp \to (\tilde{\chi}_1^\pm Z)(\tilde{\chi}_1^\mp Z) \to \tilde{\chi}_1 \tilde{\chi}_1 ZZ W^{\pm *} W^{\mp *} \tag{7}$$

occurring with a branching ratio of 3.8% (2.8%), or

$$A \to \tilde{\chi}_1^\pm \tilde{\chi}_2^\mp \to (\tilde{\chi}_1 W^{\pm *})(\tilde{\chi}_1^\mp Z) \to \tilde{\chi}_1 \tilde{\chi}_1 Z W^{\pm *} W^{\mp *} \tag{8}$$

with a decay rate of 2.7% (8.5%) for scenario 1 (scenario 2), i.e. $\tan\beta = 2.5$ (7.5).

Finally, the most frequent charged Higgs-to-electroweakino decay cascade is

$$H^\pm \to \tilde{\chi}_1 \tilde{\chi}_2^\pm \to \tilde{\chi}_1 (\tilde{\chi}_1^\pm Z) \to \tilde{\chi}_1 \tilde{\chi}_1 Z W^{\pm *} \tag{9}$$

with a rate of 6.8% (10.2%) in scenario 1 (scenario 2). Furthermore, many other possible charged Higgs-boson cascade decays yield final states with one or three W-bosons and missing transverse energy.

We stress again that searches for heavy Higgs-to-electroweakino processes are highly complementary to direct electroweakino searches, in particular in the case of a compressed electroweakino mass spectrum. While the final-state leptons in events from direct electroweakino production tend to be soft and difficult to reconstruct, this is not a problem in events where the electroweakinos originate from a heavy Higgs boson, and therefore come with a larger initial momentum. At the same time, the presence of a compressed electroweakino spectrum implies that multiple light electroweakino states are available, such that heavy Higgs-boson cascade decays via these states are possible (and even sometimes preferred, as demonstrated above), thus yielding multiple W- and Z-bosons in the final state.

For the current choice of electroweakino masses, and the example value of $M_A = 1$ TeV in Table 2, the production cross sections for direct electroweakino-pair production exceed the heavy Higgs-boson production cross sections by roughly two orders of magnitude. The leading direct electroweakino-production channels are the chargino-pair production processes $pp \to \tilde{\chi}_1^\pm \tilde{\chi}_1^\mp$ and $pp \to \tilde{\chi}_2^\pm \tilde{\chi}_2^\mp$. Due to the large difference in the rates, a dedicated search analysis

---

[12] Our scenario(s) are therefore phenomenologically very different to those considered in Ref. [153], where the final state $Z + \not{E}_T$ is regarded as the most promising search channel.

of direct electroweakino production might turn out to be more sensitive than a dedicated search for the heavy Higgs-to-electroweakino channels for this specific parameter choice, despite the more experimentally challenging kinematics in the first case. However, lifting the electroweakino-mass spectrum (see below) and/or decreasing the heavy Higgs-boson masses, while still maintaining the possibility of sizable heavy Higgs-to-electroweakino decay rates, leads to scenarios where both search strategies are sensitive and complementary.[13]

In the light of the fact that the choice of the electroweakino-mass parameters of the $M_{h,\mathrm{EFT}}^{125}(\tilde{\chi})$ scenario may already be in conflict with present LHC data (if a dedicated analyses was performed), we want to close this section with some remarks on alternative scenarios with slightly heavier electroweakinos. In Tables 1 and 2 we also include detailed information on two alternative parameter points, scenario 3 and scenario 4, in which M_1, M_2 and μ are increased from their $M_{h,\mathrm{EFT}}^{125}(\tilde{\chi})$ scenario values by 100 GeV. Again, the scenarios are distinct in the choice of $\tan\beta$ values, 2.5 and 7.5, respectively. With respect to the original $M_{h,\mathrm{EFT}}^{125}(\tilde{\chi})$ parameter points, scenario 1 and scenario 2, all electroweakino masses are simply increased by around 100 GeV. However, interestingly, there are no significant changes in the electroweakino and heavy Higgs-boson decay spectra, and our above discussion of collider signatures still holds. Also the effect of raising the electroweakino spectrum on the Higgs-boson production cross sections is below the quoted precision. On the other hand, current constraints from direct electroweakino searches are safely avoided for this alternative choice of M_1, M_2 and μ, as the production rates for direct neutralino and chargino production are significantly smaller than for the original parameter choice, see Table 1. Lastly, note that due to the increased chargino masses, the enhancement of the $h \to \gamma\gamma$ rate is less pronounced in this case, as shown in the last row of Table 2.

4.4 Comparison with the hMSSM approach

We already emphasized that the $M_{h,\mathrm{EFT}}^{125}$ scenario is the perfect candidate to assess the region of validity of the hMSSM approach [36,38,39], as it covers the same region in the $(M_A, \tan\beta)$ parameter plane, and for low values of μ/M_{SUSY} fulfills the hMSSM assumptions. As a first step, we present a comparison of the predicted heavy $\mathcal{CP}$-even Higgs-boson mass, M_H, and the (effective) $\mathcal{CP}$-even Higgs-boson mixing angle, α, in Fig. 12.[14] We only depict the range $M_A \in [150, 1000]$ GeV, since at values of $M_A \lesssim 150$ GeV

the hMSSM approach is ill-defined – the light-Higgs boson is not SM-like – and for values of $M_A > 1$ TeV the observed differences are negligible.

According to Fig. 12 the hMSSM approach provides a very good approximation to both the $\mathcal{CP}$-even Higgs-boson mixing angle and the heavy Higgs-boson mass at sufficiently large values of M_A and $\tan\beta$, where differences are at the permille level. On the other hand, at low values of $M_A \lesssim 600$ GeV and $\tan\beta \lesssim 4$, the discrepancies can reach a few percent and at very low values, i.e. in the lower-left corner, even exceed 10%, in particular for the (effective) $\mathcal{CP}$-even Higgs-boson mixing angle. Such discrepancies are slightly larger than the differences observed between the "low-$\tan\beta$-high" scenario and the hMSSM [18,33], where however lower values of M_{SUSY} were used in the low M_A and low $\tan\beta$ region. In the experimentally allowed region with $M_A \gtrsim 700$ GeV, however, the differences are well below the percent level and thus the hMSSM approach provides a decent description of the MSSM Higgs-boson sector, at least within its region of validity, i.e. for not too large values of $\tan\beta$.

The hMSSM approach assumes that the ratio μ/M_{SUSY} is small. It therefore also makes sense to compare the hMSSM approach against the $M_{h,\mathrm{EFT}}^{125}(\tilde{\chi})$ scenario, which by definition has an even smaller value of μ than the $M_{h,\mathrm{EFT}}^{125}$ scenario. On the other hand, the $M_{h,\mathrm{EFT}}^{125}(\tilde{\chi})$ scenario clearly violates one assumption of the hMSSM approach, namely it comes with light electroweakinos, which alter Higgs-boson phenomenology substantially, as discussed in detail in the previous section. Indeed, we find slightly larger differences in the prediction of the $\mathcal{CP}$-even Higgs-boson mixing angle and the heavy Higgs-boson mass than those depicted in Fig. 12, which are due to the Feynman-diagrammatic corrections induced by light electroweakinos on the Higgs-boson self energies. However again the differences are well below the permille level in the experimentally still allowed region.

5 Summary

In this paper we have proposed two new benchmark scenarios for MSSM Higgs-boson searches at the LHC, supplementing the scenarios suggested in Ref. [20]. In the scenarios proposed in Ref. [20] all SUSY particles are below or close to the TeV scale. Consequently, the parameter region of $\tan\beta \lesssim 8$ is incompatible with observations due to a too-low prediction of the SM-like Higgs-boson mass. In this work we re-opened this parameter region by allowing for squark masses of up to 10^{16} GeV, thus making it possible to reach a SM-like Higgs-boson mass of ~ 125 GeV even for low values of $\tan\beta$ and M_A (except for a region of very low values of $M_A < 200$ GeV). The presented scenarios are designed to

---

[13] A detailed analysis and comparison of the LHC sensitivity to direct electroweakino production and to heavy Higgs-to-electroweakino decays within these (and other) scenarios is left for future work.

[14] We leave a discussion of more elaborate quantities such as the Higgs-boson self-couplings and Higgs-to-Higgs decays to future work.
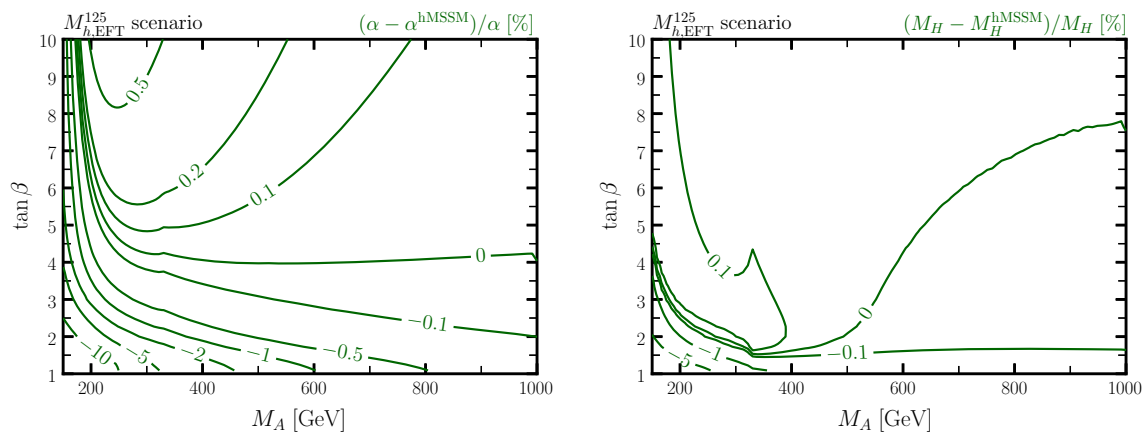
Fig. 12 *Left*: Relative difference in the prediction of the (effective) $\mathcal{CP}$-even Higgs-boson mixing angle α between the $M_{h,\text{EFT}}^{125}$ scenario and the hMSSM approach in %. *Right*: Relative difference in the prediction of the heavy $\mathcal{CP}$-even Higgs-boson mass M_H between the $M_{h,\text{EFT}}^{125}$ scenario and the hMSSM approach in %

provide guidance for experimental efforts to probe the low $\tan\beta$ region of the MSSM Higgs sector and also to motivate new LHC searches for additional heavy Higgs bosons.

Our first scenario, the "$M_{h,\text{EFT}}^{125}$" benchmark scenario, can be considered as extension of the M_h^{125} scenario [20] to low $\tan\beta$ values. In this scenario all supersymmetric particles have masses around or above the TeV scale. Consequently, the phenomenology resembles the one of a type-II 2HDM with the Higgs-boson couplings constrained to be as in the MSSM. The strongest constraint in this scenario originates from the signal-strength measurements of the SM-like Higgs boson, excluding the region of $M_A \lesssim 650$ GeV. Since the $M_{h,\text{EFT}}^{125}$ scenario fulfills the assumptions of the hMSSM approach, it is a candidate for more detailed comparisons between a complete MSSM scenario and the hMSSM approach. We presented a comparison for the predictions of the $\mathcal{CP}$-even Higgs-boson mixing angle and the heavy Higgs-boson mass and in the experimentally allowed region find discrepancies only at the permille level. On the other hand, in particular the Higgs-boson self-couplings and Higgs-to-Higgs decays need further investigations. Since they are however hardly of relevance for our work, except from small corners of the parameter space that are already ruled out by Higgs-boson signal-strength measurements, we leave them to future work.

In our second scenario, the "$M_{h,\text{EFT}}^{125}(\tilde{\chi})$" benchmark scenario, neutralinos and charginos are chosen to be light. This scenario represents an extension of the $M_h^{125}(\tilde{\chi})$ scenario [20] to low $\tan\beta$ values. The effect of low-mass charginos enhances the decay rate of the SM-like Higgs boson into photons, in particular in compressed scenarios with large gaugino-Higgsino mixing. Future precision measurements of this rate will therefore indirectly probe a significant part of the parameter space with light electroweaki-

nos. We furthermore studied in detail the possible decays of the heavy Higgs bosons into electroweakinos. While the presence of these decay modes weakens the sensitivity of LHC searches for heavy Higgs bosons decaying into SM particles, they also provide an interesting and promising new avenue for new physics searches. In fact, a signal in these channels would simultaneously reveal the presence of BSM Higgs bosons *and* supersymmetric particles. In particular, in scenarios with a compressed electroweakino mass spectrum (as chosen here), these signatures often feature multiple W- and/or Z-bosons, giving rise to multi-lepton final states, plus missing transverse energy. Moreover, as these electroweakinos originate from the decay of a heavy resonance, they can have sizable initial momentum, leading to better prospects for the reconstruction of leptons, as opposed to direct electroweakino production. LHC searches for heavy Higgs bosons decaying to electroweakinos are therefore highly complementary to existing searches for direct electroweakino production. One of the main purposes of the $M_{h,\text{EFT}}^{125}(\tilde{\chi})$ benchmark scenario (as well as the $M_h^{125}(\tilde{\chi})$ scenario [20]) is to motivate and initiate the design of dedicated searches for heavy Higgs-to-electroweakino decay signatures.

Data Availability Statement This manuscript has data included as electronic supplementary material.

to the original author(s) and the source, provide a link to the Creative Commons license, and indicate if changes were made.

Funded by SCOAP³.

References

1. ATLAS Collaboration, G. Aad et al., Observation of a new particle in the search for the standard model Higgs boson with the ATLAS detector at the LHC. Phys. Lett. B **716**, 1–29 (2012). arXiv:1207.7214 [hep-ex]
2. CMS Collaboration, S. Chatrchyan et al., Observation of a new boson at a mass of 125 GeV with the CMS experiment at the LHC. Phys. Lett. B **716**, 30–61 (2012). arXiv:1207.7235 [hep-ex]
3. ATLAS, CMS Collaboration, G. Aad et al., Combined measurement of the Higgs boson mass in pp collisions at $\sqrt{s} = 7$ and 8 TeV with the ATLAS and CMS experiments. Phys. Rev. Lett. **114**, 191803 (2015). arXiv:1503.07589 [hep-ex]
4. ATLAS, CMS Collaboration, G. Aad et al., Measurements of the Higgs boson production and decay rates and constraints on its couplings from a combined ATLAS and CMS analysis of the LHC pp collision data at $\sqrt{s} = 7$ and 8 TeV. JHEP **08**, 045 (2016). arXiv:1606.02266 [hep-ex]
5. H.P. Nilles, Supersymmetry, supergravity and particle physics. Phys. Rep. **110**, 1–162 (1984)
6. H.E. Haber, G.L. Kane, The search for supersymmetry: probing physics beyond the standard model. Phys. Rep. **117**, 75–263 (1985)
7. J.F. Gunion, H.E. Haber, Higgs bosons in supersymmetric models. 1. Nucl. Phys. B **272**, 1 (1986). [Erratum: Nucl. Phys. B **402**, 567 (1993)]
8. S. Heinemeyer, O. Stål, G. Weiglein, Interpreting the LHC Higgs search results in the MSSM. Phys. Lett. B **710**, 201–206 (2012). arXiv:1112.3026 [hep-ph]
9. M. Drees, A supersymmetric explanation of the excess of Higgs-like events at the LHC and at LEP. Phys. Rev. D **86**, 115018 (2012). arXiv:1210.6507 [hep-ph]
10. P. Bechtle, S. Heinemeyer, O. Stål, T. Stefaniak, G. Weiglein, L. Zeune, MSSM interpretations of the LHC discovery: light or heavy Higgs? Eur. Phys. J. C **73**(4), 2354 (2013). arXiv:1211.1955 [hep-ph]
11. P. Bechtle, H.E. Haber, S. Heinemeyer, O. Stål, T. Stefaniak, G. Weiglein, L. Zeune, The light and heavy Higgs interpretation of the MSSM. Eur. Phys. J. C **77**(2), 67 (2017). arXiv:1608.00638 [hep-ph]
12. H.E. Haber, S. Heinemeyer, T. Stefaniak, The impact of two-loop effects on the scenario of MSSM Higgs alignment without decoupling. Eur. Phys. J. C **77**(11), 742 (2017). arXiv:1708.04416 [hep-ph]
13. P. Draper, H. Rzehak, A review of Higgs mass calculations in supersymmetric models. Phys. Rep. **619**, 1–24 (2016). arXiv:1601.01890 [hep-ph]
14. M. Carena, S. Heinemeyer, C.E.M. Wagner, G. Weiglein, Suggestions for improved benchmark scenarios for Higgs boson searches at LEP-2, in Workshop on New Theoretical Developments for Higgs Physics at LEP-2 Geneva, Switzerland, October 27, 1999 (1999). arXiv:hep-ph/9912223 [hep-ph]
15. M. Carena, S. Heinemeyer, C.E.M. Wagner, G. Weiglein, Suggestions for benchmark scenarios for MSSM Higgs boson searches at hadron colliders. Eur. Phys. J. C **26**, 601–607 (2003). arXiv:hep-ph/0202167 [hep-ph]
16. M. Carena, S. Heinemeyer, O. Stål, C.E.M. Wagner, G. Weiglein, MSSM Higgs boson searches at the LHC: benchmark scenarios after the discovery of a Higgs-like particle. Eur. Phys. J. C **73**(9), 2552 (2013). arXiv:1302.7033 [hep-ph]
17. M. Carena, J.R. Ellis, A. Pilaftsis, C.E.M. Wagner, CP violating MSSM Higgs bosons in the light of LEP-2. Phys. Lett. B **495**, 155–163 (2000). arXiv:hep-ph/0009212 [hep-ph]
18. E. Bagnaschi, F. Frensch, S. Heinemeyer, G. Lee, S.R. Liebler, M. Mühlleitner, A.R. McCarn, J. Quevillon, N. Rompotis, P. Slavich, M. Spira, C. Wagner, R. Wolf, Benchmark scenarios for low tan β in the MSSM Tech. Rep. LHCHXSWG-2015-002, CERN, Geneva, Aug (2015). https://cds.cern.ch/record/2039911
19. M. Carena, J. Ellis, J.S. Lee, A. Pilaftsis, C.E.M. Wagner, CP violation in heavy MSSM Higgs scenarios. JHEP **02**, 123 (2016). arXiv:1512.00437 [hep-ph]
20. H. Bahl, E. Fuchs, T. Hahn, S. Heinemeyer, S. Liebler, S. Patel, P. Slavich, T. Stefaniak, C.E.M. Wagner, G. Weiglein, MSSM Higgs boson searches at the LHC: benchmark scenarios for run 2 and beyond. arXiv:1808.07542 [hep-ph]
21. ATLAS Collaboration, M. Aaboud et al., Search for additional heavy neutral Higgs and gauge bosons in the ditau final state produced in 36 fb^{-1} of pp collisions at $\sqrt{s} = 13$ TeV with the ATLAS detector. JHEP **01**, 055 (2018). arXiv:1709.07242 [hep-ex]
22. CMS Collaboration, A.M. Sirunyan et al., Search for additional neutral MSSM Higgs bosons in the $\tau\tau$ final state in proton–proton collisions at $\sqrt{s} = 13$ TeV. JHEP **09**, 007 (2018). arXiv:1803.06553 [hep-ex]
23. G.F. Giudice, A. Strumia, Probing high-scale and split supersymmetry with Higgs mass measurements. Nucl. Phys. B **858**, 63–83 (2012). arXiv:1108.6077 [hep-ph]
24. T. Hahn, S. Heinemeyer, W. Hollik, H. Rzehak, G. Weiglein, High-precision predictions for the light CP-even Higgs boson mass of the minimal supersymmetric standard model. Phys. Rev. Lett. **112**(14), 141801 (2014). arXiv:1312.4937 [hep-ph]
25. P. Draper, G. Lee, C.E.M. Wagner, Precise estimates of the Higgs mass in heavy supersymmetry. Phys. Rev. D **89**(5), 055023 (2014). arXiv:1312.5743 [hep-ph]
26. E. Bagnaschi, G.F. Giudice, P. Slavich, A. Strumia, Higgs mass and unnatural supersymmetry. JHEP **09**, 092 (2014). arXiv:1407.4081 [hep-ph]
27. J. Pardo Vega, G. Villadoro, SusyHD: Higgs mass determination in supersymmetry. JHEP **07**, 159 (2015). arXiv:1504.05200 [hep-ph]
28. H. Bahl, W. Hollik, Precise prediction for the light MSSM Higgs boson mass combining effective field theory and fixed-order calculations. Eur. Phys. J. C **76**(9), 499 (2016). arXiv:1608.01880 [hep-ph]
29. E. Bagnaschi, J. Pardo Vega, P. Slavich, Improved determination of the Higgs mass in the MSSM with heavy superpartners. Eur. Phys. J. C **77**(5), 334 (2017). arXiv:1703.08166 [hep-ph]
30. H. Bahl, S. Heinemeyer, W. Hollik, G. Weiglein, Reconciling EFT and hybrid calculations of the light MSSM Higgs-boson mass. Eur. Phys. J. C **78**(1), 57 (2018). arXiv:1706.00346 [hep-ph]
31. R.V. Harlander, J. Klappert, A.D. Ochoa Franco, A. Voigt, The light CP-even MSSM Higgs mass resummed to fourth logarithmic order. Eur. Phys. J. C **78**(10), 874 (2018). arXiv:1807.03509 [hep-ph]
32. H.E. Haber, R. Hempfling, The renormalization group improved Higgs sector of the minimal supersymmetric model. Phys. Rev. D **48**, 4280–4309 (1993). arXiv:hep-ph/9307201 [hep-ph]
33. G. Lee, C.E.M. Wagner, Higgs bosons in heavy supersymmetry with an intermediate m$_A$. Phys. Rev. D **92**(7), 075032 (2015). arXiv:1508.00576 [hep-ph]
34. P. Athron, M. Bach, D. Harries, T. Kwasnitza, J-h Park, D. Stöckinger, A. Voigt, J. Ziebell, FlexibleSUSY 2.0: extensions to investigate the phenomenology of SUSY and non-SUSY models. Comput. Phys. Commun. **230**, 145–217 (2018). arXiv:1710.03760 [hep-ph]

35. M. Gabelmann, M. Mühlleitner, F. Staub, Automatised matching between two scalar sectors at the one-loop level. Eur. Phys. J. C **79**(2), 163 (2019). https://doi.org/10.1140/epjc/s10052-019-6570-5. arXiv:1810.12326 [hep-ph]

36. A. Djouadi, J. Quevillon, The MSSM Higgs sector at a high M_{SUSY}: reopening the low $\tan\beta$ regime and heavy Higgs searches. JHEP **10**, 028 (2013). arXiv:1304.1787 [hep-ph]

37. L. Maiani, A.D. Polosa, V. Riquer, Bounds to the Higgs sector masses in minimal supersymmetry from LHC data. Phys. Lett. B **724**, 274–277 (2013). arXiv:1305.2172 [hep-ph]

38. A. Djouadi, L. Maiani, G. Moreau, A. Polosa, J. Quevillon, V. Riquer, The post-Higgs MSSM scenario: habemus MSSM? Eur. Phys. J. C **73**, 2650 (2013). arXiv:1307.5205 [hep-ph]

39. A. Djouadi, L. Maiani, A. Polosa, J. Quevillon, V. Riquer, Fully covering the MSSM Higgs sector at the LHC. JHEP **06**, 168 (2015). arXiv:1502.05653 [hep-ph]

40. S. Liebler, M. Mühlleitner, M. Spira, M. Stadelmaier, The hMSSM approach for Higgs self-couplings revisited. Eur. Phys. J. C **79**(1), 65 (2019). https://doi.org/10.1140/epjc/s10052-019-6594-x. arXiv:1810.10979 [hep-ph]

41. S. Heinemeyer, W. Hollik, G. Weiglein, FeynHiggs: a program for the calculation of the masses of the neutral CP even Higgs bosons in the MSSM. Comput. Phys. Commun. **124**, 76–89 (2000). arXiv:hep-ph/9812320 [hep-ph]

42. S. Heinemeyer, W. Hollik, G. Weiglein, The masses of the neutral CP-even Higgs bosons in the MSSM: accurate analysis at the two loop level. Eur. Phys. J. C **9**, 343–366 (1999). arXiv:hep-ph/9812472 [hep-ph]

43. G. Degrassi, S. Heinemeyer, W. Hollik, P. Slavich, G. Weiglein, Towards high precision predictions for the MSSM Higgs sector. Eur. Phys. J. C **28**, 133–143 (2003). arXiv:hep-ph/0212020 [hep-ph]

44. M. Frank, T. Hahn, S. Heinemeyer, W. Hollik, H. Rzehak, G. Weiglein, The Higgs boson masses and mixings of the complex MSSM in the Feynman-diagrammatic approach. JHEP **02**, 047 (2007). arXiv:hep-ph/0611326 [hep-ph]

45. H. Bahl, T. Hahn, S. Heinemeyer, W. Hollik, S. Paßehr, H. Rzehak, G. Weiglein, Precision calculations in the MSSM Higgs-boson sector with FeynHiggs 2.14. arXiv:1811.09073 [hep-ph]

46. H. Bahl, W. Hollik, Precise prediction of the MSSM Higgs boson masses for low M_A. JHEP **07**, 182 (2018). arXiv:1805.00867 [hep-ph]

47. R.V. Harlander, S. Liebler, H. Mantler, SuSHi: a program for the calculation of Higgs production in gluon fusion and bottom-quark annihilation in the standard model and the MSSM. Comput. Phys. Commun. **184**, 1605–1617 (2013). arXiv:1212.3249 [hep-ph]

48. R.V. Harlander, S. Liebler, H. Mantler, SuSHi Bento: beyond NNLO and the heavy-top limit. Comput. Phys. Commun. **212**, 239–257 (2017). arXiv:1605.03190 [hep-ph]

49. S. Forte, D. Napoletano, M. Ubiali, Higgs production in bottom-quark fusion: matching beyond leading order. Phys. Lett. B **763**, 190–196 (2016). arXiv:1607.00389 [hep-ph]

50. S. Forte, D. Napoletano, M. Ubiali, Higgs production in bottom-quark fusion in a matched scheme. Phys. Lett. B **751**, 331–337 (2015). arXiv:1508.01529 [hep-ph]

51. M. Bonvini, A.S. Papanastasiou, F.J. Tackmann, Matched predictions for the $b\bar{b}H$ cross section at the 13 TeV LHC. JHEP **10**, 053 (2016). arXiv:1605.01733 [hep-ph]

52. M. Bonvini, A.S. Papanastasiou, F.J. Tackmann, Resummation and matching of b-quark mass effects in $b\bar{b}H$ production. JHEP **11**, 196 (2015). arXiv:1508.03288 [hep-ph]

53. P. Bechtle, O. Brein, S. Heinemeyer, G. Weiglein, K.E. Williams, HiggsBounds: confronting arbitrary Higgs sectors with exclusion bounds from LEP and the Tevatron. Comput. Phys. Commun. **181**, 138–167 (2010). arXiv:0811.4169 [hep-ph]

54. P. Bechtle, O. Brein, S. Heinemeyer, G. Weiglein, K.E. Williams, HiggsBounds 2.0.0: confronting neutral and charged higgs sector predictions with exclusion bounds from LEP and the Tevatron. Comput. Phys. Commun. **182**, 2605–2631 (2011). arXiv:1102.1898 [hep-ph]

55. P. Bechtle, O. Brein, S. Heinemeyer, O. Stål, T. Stefaniak, G. Weiglein, K.E. Williams, HiggsBounds-4: improved tests of extended Higgs sectors against exclusion bounds from LEP, the Tevatron and the LHC. Eur. Phys. J. C **74**(3), 2693 (2014). arXiv:1311.0055 [hep-ph]

56. P. Bechtle, S. Heinemeyer, O. Stål, T. Stefaniak, G. Weiglein, Applying exclusion likelihoods from LHC searches to extended Higgs sectors. Eur. Phys. J. C **75**(9), 421 (2015). arXiv:1507.06706 [hep-ph]

57. P. Bechtle, S. Heinemeyer, O. Stål, T. Stefaniak, G. Weiglein, *HiggsSignals*: confronting arbitrary Higgs sectors with measurements at the Tevatron and the LHC. Eur. Phys. J. C **74**(2), 2711 (2014). arXiv:1305.1933 [hep-ph]

58. A.V. Bednyakov, On three-loop RGE for the Higgs sector of 2HDM. JHEP **11**, 154 (2018). arXiv:1809.04527 [hep-ph]

59. I. Schienbein, F. Staub, T. Steudtner, K. Svirina, Revisiting RGEs for general gauge theories. Nucl. Phys. B **939**, 1–48 (2019). https://doi.org/10.1016/j.nuclphysb.2018.12.001. arXiv:1809.06797 [hep-ph]

60. P.H. Chankowski, S. Pokorski, J. Rosiek, Complete on-shell renormalization scheme for the minimal supersymmetric Higgs sector. Nucl. Phys. B **423**, 437–496 (1994). arXiv:hep-ph/9303309 [hep-ph]

61. A. Dabelstein, Fermionic decays of neutral MSSM Higgs bosons at the one loop level. Nucl. Phys. B **456**, 25–56 (1995). arXiv:hep-ph/9503443 [hep-ph]

62. D.M. Pierce, J.A. Bagger, K.T. Matchev, R.-J. Zhang, Precision corrections in the minimal supersymmetric standard model. Nucl. Phys. B **491**, 3–67 (1997). arXiv:hep-ph/9606211 [hep-ph]

63. E. Bagnaschi, F. Brümmer, W. Buchmüller, A. Voigt, G. Weiglein, Vacuum stability and supersymmetry at high scales with two Higgs doublets. JHEP **03**, 158 (2016). arXiv:1512.07761 [hep-ph]

64. S. Liebler, S. Patel, G. Weiglein, Phenomenology of on-shell Higgs production in the MSSM with complex parameters. Eur. Phys. J. C **77**(5), 305 (2017). arXiv:1611.09308 [hep-ph]

65. E. Fuchs, G. Weiglein, Breit–Wigner approximation for propagators of mixed unstable states. JHEP **09**, 079 (2017). arXiv:1610.06193 [hep-ph]

66. H. Bahl, Pole mass determination in presence of heavy particles. JHEP **02**, 121 (2019). https://doi.org/10.1007/JHEP02(2019)121. arXiv:1812.06452 [hep-ph]

67. M. Spira, A. Djouadi, D. Graudenz, P.M. Zerwas, Higgs boson production at the LHC. Nucl. Phys. B **453**, 17–82 (1995). arXiv:hep-ph/9504378 [hep-ph]

68. R. Harlander, P. Kant, Higgs production and decay: analytic results at next-to-leading order QCD. JHEP **12**, 015 (2005). arXiv:hep-ph/0509189 [hep-ph]

69. R.V. Harlander, W.B. Kilgore, Next-to-next-to-leading order Higgs production at hadron colliders. Phys. Rev. Lett. **88**, 201801 (2002). arXiv:hep-ph/0201206 [hep-ph]

70. C. Anastasiou, K. Melnikov, Higgs boson production at hadron colliders in NNLO QCD. Nucl. Phys. B **646**, 220–256 (2002). arXiv:hep-ph/0207004 [hep-ph]

71. V. Ravindran, J. Smith, W.L. van Neerven, NNLO corrections to the total cross-section for Higgs boson production in hadron hadron collisions. Nucl. Phys. B **665**, 325–366 (2003). arXiv:hep-ph/0302135 [hep-ph]

72. R.V. Harlander, W.B. Kilgore, Production of a pseudoscalar Higgs boson at hadron colliders at next-to-next-to leading order. JHEP **10**, 017 (2002). arXiv:hep-ph/0208096 [hep-ph]

73. C. Anastasiou, K. Melnikov, Pseudoscalar Higgs boson production at hadron colliders in NNLO QCD. Phys. Rev. D **67**, 037501 (2003). arXiv:hep-ph/0208115 [hep-ph]

74. C. Anastasiou, C. Duhr, F. Dulat, E. Furlan, T. Gehrmann, F. Herzog, B. Mistlberger, Higgs boson gluon fusion production beyond threshold in N^3LO QCD. JHEP **03**, 091 (2015). arXiv:1411.3584 [hep-ph]

75. C. Anastasiou, C. Duhr, F. Dulat, E. Furlan, F. Herzog, B. Mistlberger, Soft expansion of double-real-virtual corrections to Higgs production at N^{3}LO. JHEP **08**, 051 (2015). arXiv:1505.04110 [hep-ph]

76. C. Anastasiou, C. Duhr, F. Dulat, E. Furlan, T. Gehrmann, F. Herzog, A. Lazopoulos, B. Mistlberger, High precision determination of the gluon fusion Higgs boson cross-section at the LHC. JHEP **05**, 058 (2016). arXiv:1602.00695 [hep-ph]

77. LHC Higgs Cross Section Working Group Collaboration, D. de Florian et al., Handbook of LHC Higgs cross sections: 4. Deciphering the nature of the Higgs sector. arXiv:1610.07922 [hep-ph]

78. B. Mistlberger, Higgs boson production at hadron colliders at N^{3}LO in QCD. JHEP **05**, 028 (2018). arXiv:1802.00833 [hep-ph]

79. U. Aglietti, R. Bonciani, G. Degrassi, A. Vicini, Two loop light fermion contribution to Higgs production and decays. Phys. Lett. B **595**, 432–441 (2004). arXiv:hep-ph/0404071 [hep-ph]

80. R. Bonciani, G. Degrassi, A. Vicini, On the generalized harmonic polylogarithms of one complex variable. Comput. Phys. Commun. **182**, 1253–1264 (2011). arXiv:1007.1891 [hep-ph]

81. J. Butterworth et al., PDF4LHC recommendations for LHC run II. J. Phys. G **43**, 023001 (2016). arXiv:1510.03865 [hep-ph]

82. R. Harlander, M. Krämer, M. Schumacher, Bottom-quark associated Higgs-boson production: reconciling the four- and five-flavour scheme approach. arXiv:1112.3478 [hep-ph]

83. R.V. Harlander, W.B. Kilgore, Higgs boson production in bottom quark fusion at next-to-next-to leading order. Phys. Rev. D **68**, 013001 (2003). arXiv:hep-ph/0304035 [hep-ph]

84. S. Dittmaier, M. Krämer, M. Spira, Higgs radiation off bottom quarks at the Tevatron and the CERN LHC. Phys. Rev. D **70**, 074010 (2004). arXiv:hep-ph/0309204 [hep-ph]

85. S. Dawson, C.B. Jackson, L. Reina, D. Wackeroth, Exclusive Higgs boson production with bottom quarks at hadron colliders. Phys. Rev. D **69**, 074027 (2004). arXiv:hep-ph/0311067 [hep-ph]

86. E. Bagnaschi, R.V. Harlander, S. Liebler, H. Mantler, P. Slavich, A. Vicini, Towards precise predictions for Higgs-boson production in the MSSM. JHEP **06**, 167 (2014). arXiv:1404.0327 [hep-ph]

87. E.L. Berger, T. Han, J. Jiang, T. Plehn, Associated production of a top quark and a charged Higgs boson. Phys. Rev. D **71**, 115012 (2005). arXiv:hep-ph/0312286 [hep-ph]

88. S. Dittmaier, M. Krämer, M. Spira, M. Walser, Charged-Higgs-boson production at the LHC: NLO supersymmetric QCD corrections. Phys. Rev. D **83**, 055005 (2011). arXiv:0906.2648 [hep-ph]

89. M. Flechl, R. Klees, M. Krämer, M. Spira, M. Ubiali, Improved cross-section predictions for heavy charged Higgs boson production at the LHC. Phys. Rev. D **91**(7), 075015 (2015). arXiv:1409.5615 [hep-ph]

90. C. Degrande, M. Ubiali, M. Wiesemann, M. Zaro, Heavy charged Higgs boson production at the LHC. JHEP **10**, 145 (2015). arXiv:1507.02549 [hep-ph]

91. C. Degrande, R. Frederix, V. Hirschi, M. Ubiali, M. Wiesemann, M. Zaro, Accurate predictions for charged Higgs production: closing the $m_{H^\pm} \sim m_t$ window. Phys. Lett. B **772**, 87–92 (2017). arXiv:1607.05291 [hep-ph]

92. CMS Collaboration, Search for additional neutral Higgs bosons decaying to a pair of tau leptons in pp collisions at $\sqrt{s} = 7$ and 8 TeV. CMS-PAS-HIG-14-029 (2015)

93. ATLAS Collaboration, G. Aad et al., Search for an additional, heavy Higgs boson in the $H \to ZZ$ decay channel at $\sqrt{s} = 8$ TeV in pp collision data with the ATLAS detector. Eur. Phys. J. C **76**(1), 45 (2016). arXiv:1507.05930 [hep-ex]

94. ATLAS Collaboration, M. Aaboud et al., Search for heavy ZZ resonances in the $\ell^+\ell^-\ell^+\ell^-$ and $\ell^+\ell^-\nu\bar{\nu}$ final states using proton–proton collisions at $\sqrt{s} = 13$ TeV with the ATLAS detector. Eur. Phys. J. C **78**(4), 293 (2018). arXiv:1712.06386 [hep-ex]

95. CMS Collaboration, V. Khachatryan et al., Search for a Higgs boson in the mass range from 145 to 1000 GeV decaying to a pair of W or Z bosons. JHEP **10**, 144 (2015). arXiv:1504.00936 [hep-ex]

96. CMS Collaboration, A.M. Sirunyan et al., Search for a new scalar resonance decaying to a pair of Z bosons in proton-proton collisions at $\sqrt{s} = 13$ TeV. JHEP **06**, 127 (2018). arXiv:1804.01939 [hep-ex]

97. ATLAS Collaboration, M. Aaboud et al., Search for resonant and nonresonant Higgs boson pair production in the $b\bar{b}\tau^+\tau^-$ decay channel in pp collisions at $\sqrt{s} = 13$ TeV with the ATLAS detector. Phys. Rev. Lett. **121**(19), 191801 (2018). arXiv:1808.00336 [hep-ex]

98. CMS Collaboration, A.M. Sirunyan et al., Search for Higgs boson pair production in events with two bottom quarks and two tau leptons in proton-proton collisions at $\sqrt{s} = 13$ TeV. Phys. Lett. B **778**, 101–127 (2018). https://doi.org/10.1016/j.physletb.2018.01.001. arXiv:1707.02909 [hep-ex]

99. CMS Collaboration, A.M. Sirunyan et al., Search for resonant and nonresonant Higgs boson pair production in the bb̄ℓνℓν final state in proton-proton collisions at $\sqrt{s} = 13$ TeV. JHEP **01**, 054 (2018). arXiv:1708.04188 [hep-ex]

100. CMS Collaboration, Search for pair production of Higgs bosons in the two tau leptons and two bottom quarks final state using proton-proton collisions at $\sqrt{s} = 13$ TeV. CMS-PAS-HIG-17-002 (2017)

101. CMS Collaboration, A.M. Sirunyan et al., Combination of searches for Higgs boson pair production in proton-proton collisions at $\sqrt{s} = 13$ TeV. arXiv:1811.09689 [hep-ex]

102. CMS Collaboration, V. Khachatryan et al., Search for a charged Higgs boson in pp collisions at $\sqrt{s} = 8$ TeV. JHEP **11**, 018 (2015). arXiv:1508.07774 [hep-ex]

103. CMS Collaboration, Search for charged Higgs bosons with the $H^\pm \to \tau^\pm \nu_\tau$ decay channel in the fully hadronic final state at $\sqrt{s} = 13$ TeV. CMS-PAS-HIG-16-031 (2016)

104. ATLAS Collaboration, G. Aad et al., Search for charged Higgs bosons decaying via $H^\pm \to \tau^\pm \nu$ in fully hadronic final states using pp collision data at $\sqrt{s} = 8$ TeV with the ATLAS detector. JHEP **03**, 088 (2015). arXiv:1412.6663 [hep-ex]

105. ATLAS Collaboration, M. Aaboud et al., Search for charged Higgs bosons decaying via $H^\pm \to \tau^\pm \nu_\tau$ in the τ+jets and τ + lepton final states with 36 fb^{-1} of pp collision data recorded at $\sqrt{s} = 13$ TeV with the ATLAS experiment. JHEP **09**, 139 (2018). https://doi.org/10.1007/JHEP09(2018)139. arXiv:1807.07915 [hep-ex]

106. ATLAS Collaboration, G. Aad et al., Search for charged Higgs bosons in the $H^\pm \to tb$ decay channel in pp collisions at $\sqrt{s} = 8$ TeV using the ATLAS detector. JHEP **03**, 127 (2016). arXiv:1512.03704 [hep-ex]

107. ATLAS Collaboration, M. Aaboud et al., Search for charged Higgs bosons decaying into top and bottom quarks at $\sqrt{s} = 13$ TeV with the ATLAS detector. JHEP **11**, 085 (2018). arXiv:1808.03599 [hep-ex]

108. ATLAS Collaboration, Measurements of the Higgs boson production cross section via vector boson fusion and associated WH production in the $WW^* \to \ell\nu\ell\nu$ decay mode with the ATLAS detector at $\sqrt{s} = 13$ TeV. ATLAS-CONF-2016-112 (2016)

109. ATLAS Collaboration, Measurement of gluon fusion and vector boson fusion Higgs boson production cross-sections in the $H \to WW^* \to e\nu\mu\nu$ decay channel in pp collisions at $\sqrt{s} = 13$ TeV with the ATLAS detector. ATLAS-CONF-2018-004 (2018)

110. ATLAS Collaboration, M. Aaboud et al., Evidence for the $H \rightarrow b\bar{b}$ decay with the ATLAS detector. JHEP **12**, 024 (2017). arXiv:1708.03299 [hep-ex]

111. ATLAS Collaboration, M. Aaboud et al., Measurement of the Higgs boson coupling properties in the $H \rightarrow ZZ^* \rightarrow 4\ell$ decay channel at $\sqrt{s} = 13$ TeV with the ATLAS detector. JHEP **03**, 095 (2018). arXiv:1712.02304 [hep-ex]

112. ATLAS Collaboration, M. Aaboud et al., Evidence for the associated production of the Higgs boson and a top quark pair with the ATLAS detector. Phys. Rev. D **97**(7), 072003 (2018). arXiv:1712.08891 [hep-ex]

113. ATLAS Collaboration, M. Aaboud et al., Search for the standard model Higgs boson produced in association with top quarks and decaying into a $b\bar{b}$ pair in pp collisions at $\sqrt{s} = 13$ TeV with the ATLAS detector. Phys. Rev. D **97**(7), 072016 (2018). arXiv:1712.08895 [hep-ex]

114. ATLAS Collaboration, M. Aaboud et al., Measurements of Higgs boson properties in the diphoton decay channel with 36 fb^{-1} of pp collision data at $\sqrt{s} = 13$ TeV with the ATLAS detector. Phys. Rev. D **98**, 052005 (2018). https://doi.org/10.1103/PhysRevD.98.052005. arXiv:1802.04146 [hep-ex]

115. CMS Collaboration, Measurements of properties of the Higgs boson in the diphoton decay channel with the full 2016 data set. CMS-PAS-HIG-16-040 (2017)

116. CMS Collaboration, A.M. Sirunyan et al., Measurements of properties of the Higgs boson decaying into the four-lepton final state in pp collisions at $\sqrt{s} = 13$ TeV. JHEP **11**, 047 (2017). arXiv:1706.09936 [hep-ex]

117. CMS Collaboration, A.M. Sirunyan et al., Observation of the Higgs boson decay to a pair of τ leptons with the CMS detector. Phys. Lett. B **779**, 283–316 (2018). arXiv:1708.00373 [hep-ex]

118. CMS Collaboration, A. M. Sirunyan et al., Inclusive search for a highly boosted Higgs boson decaying to a bottom quark-antiquark pair. Phys. Rev. Lett. **120**(7), 071802 (2018). arXiv:1709.05543 [hep-ex]

119. CMS Collaboration, A.M. Sirunyan et al., Evidence for the Higgs boson decay to a bottom quark–antiquark pair. Phys. Lett. B **780**, 501–532 (2018). arXiv:1709.07497 [hep-ex]

120. CMS Collaboration, A. M. Sirunyan et al., Evidence for associated production of a Higgs boson with a top quark pair in final states with electrons, muons, and hadronically decaying τ leptons at $\sqrt{s} = 13$ TeV. JHEP **08**, 066 (2018). https://doi.org/10.1007/JHEP08(2018)066. arXiv:1803.05485 [hep-ex]

121. CMS Collaboration, A.M. Sirunyan et al., Search for t$\bar{t}$H production in the all-jet final state in proton-proton collisions at $\sqrt{s} = 13$ TeV. JHEP **06**, 101 (2018). arXiv:1803.06986 [hep-ex]

122. CMS Collaboration, A.M. Sirunyan et al., Search for t$\bar{t}$H production in the $H \rightarrow b\bar{b}$ decay channel with leptonic t$\bar{t}$ decays in proton–proton collisions at $\sqrt{s} = 13$. TeV. JHEP **03**, 026 (2019). https://doi.org/10.1007/JHEP03(2019)026. arXiv:1804.03682 [hep-ex]

123. CMS Collaboration, A.M. Sirunyan et al., Measurements of properties of the Higgs boson decaying to a W boson pair in pp collisions at $\sqrt{s} = 13$ TeV. Phys. Lett. B **791**, 96 (2019). https://doi.org/10.1016/j.physletb.2018.12.073. arXiv:1806.05246 [hep-ex]

124. CMS Collaboration, A.M. Sirunyan et al., Search for the Higgs boson decaying to two muons in proton-proton collisions at $\sqrt{s} = 13$ TeV. Phys. Rev. Lett. **122**(2), 021801 (2019). https://doi.org/10.1103/PhysRevLett.122.021801. arXiv:1807.06325 [hep-ex]

125. Particle Data Group Collaboration, C. Patrignani et al., Review of particle physics. Chin. Phys. **C40**(10), 100001 (2016)

126. ATLAS Collaboration, M. Aaboud et al., Search for squarks and gluinos in events with an isolated lepton, jets, and missing transverse momentum at $\sqrt{s} = 13$ TeV with the ATLAS detector. Phys. Rev. D **96**(11), 112010 (2017). arXiv:1708.08232 [hep-ex]

127. ATLAS Collaboration, M. Aaboud et al., Search for squarks and gluinos in final states with jets and missing transverse momentum using 36 fb^{-1} of $\sqrt{s} = 13$ TeV pp collision data with the ATLAS detector. Phys. Rev. D **97**(11), 112001 (2018). https://doi.org/10.1103/PhysRevD.97.112001. arXiv:1712.02332 [hep-ex]

128. CMS Collaboration, A. M. Sirunyan et al., Search for supersymmetry in multijet events with missing transverse momentum in proton-proton collisions at 13 TeV. Phys. Rev. D **96**(3), 032003 (2017). arXiv:1704.07781 [hep-ex]

129. CMS Collaboration, A.M. Sirunyan et al., Search for new phenomena with the M_{T2} variable in the all-hadronic final state produced in proton–proton collisions at $\sqrt{s} = 13$ TeV. Eur. Phys. J. C **77**(10), 710 (2017). arXiv:1705.04650 [hep-ex]

130. CMS Collaboration, A.M. Sirunyan et al., Search for natural and split supersymmetry in proton–proton collisions at $\sqrt{s} = 13$ TeV in final states with jets and missing transverse momentum. JHEP **05**, 025 (2018). https://doi.org/10.1007/JHEP05(2018)025. arXiv:1802.02110 [hep-ex]

131. ATLAS Collaboration, M. Aaboud et al., Search for supersymmetry in final states with two same-sign or three leptons and jets using 36 fb^{-1} of $\sqrt{s} = 13$ TeV pp collision data with the ATLAS detector. JHEP **09**, 084 (2017). arXiv:1706.03731 [hep-ex]

132. G. Bhattacharyya, D. Das, M.J. Pérez, I. Saha, A. Santamaria, O. Vives, Can measurements of 2HDM parameters provide hints for high scale supersymmetry? Phys. Rev. D **97**(9), 095018 (2018). arXiv:1712.00791 [hep-ph]

133. B.C. Allanach, A. Djouadi, J.L. Kneur, W. Porod, P. Slavich, Precise determination of the neutral Higgs boson masses in the MSSM. JHEP **09**, 044 (2004). arXiv:hep-ph/0406166 [hep-ph]

134. ATLAS Collaboration, M. Aaboud et al., Search for heavy Higgs bosons A/H decaying to a top quark pair in pp collisions at $\sqrt{s} = 8$ TeV with the ATLAS detector. Phys. Rev. Lett. **119**(19), 191803 (2017). arXiv:1707.06025 [hep-ex]

135. K.J.F. Gaemers, F. Hoogeveen, Higgs production and decay into heavy flavors with the gluon fusion mechanism. Phys. Lett. **146B**, 347–349 (1984)

136. D. Dicus, A. Stange, S. Willenbrock, Higgs decay to top quarks at hadron colliders. Phys. Lett. B **333**, 126–131 (1994). arXiv:hep-ph/9404359 [hep-ph]

137. S. Moretti, D.A. Ross, On the top-antitop invariant mass spectrum at the LHC from a Higgs boson signal perspective. Phys. Lett. B **712**, 245–249 (2012). arXiv:1203.3746 [hep-ph]

138. R. Frederix, F. Maltoni, Top pair invariant mass distribution: a window on new physics. JHEP **01**, 047 (2009). arXiv:0712.2355 [hep-ph]

139. B. Hespel, F. Maltoni, E. Vryonidou, Signal background interference effects in heavy scalar production and decay to a top-anti-top pair. JHEP **10**, 016 (2016). arXiv:1606.04149 [hep-ph]

140. A. Djouadi, J. Ellis, A. Popov, J. Quevillon, Interference effects in $t\bar{t}$ production at the LHC as a window on new physics. arXiv:1901.03417 [hep-ph]

141. D. Denegri, V. Drollinger, R. Kinnunen, K. Lassila-Perini, S. Lehti, F. Moortgat, A. Nikitenko, S. Slabospitsky, N. Stepanov, Summary of the CMS discovery potential for the MSSM SUSY Higgses. arXiv:hep-ph/0112045 [hep-ph]

142. F. Moortgat, S. Abdullin, D. Denegri, Observability of MSSM Higgs bosons via sparticle decay modes in CMS. arXiv:hep-ph/0112046 [hep-ph]

143. S. Abdullin et al., Summary of the CMS potential for the Higgs boson discovery. Eur. Phys. J. C **39S2**, 41–61 (2005)

144. E. Arganda, J.L. Diaz-Cruz, A. Szynkman, Decays of H^0/A^0 in supersymmetric scenarios with heavy sfermions. Eur. Phys. J. C **73**(4), 2384 (2013). arXiv:1211.0163 [hep-ph]

145. E. Arganda, J. Lorenzo Diaz-Cruz, A. Szynkman, Slim SUSY. Phys. Lett. B **722**, 100–106 (2013). arXiv:1301.0708 [hep-ph]

146. N. Craig, F. D'Eramo, P. Draper, S. Thomas, H. Zhang, The hunt for the rest of the Higgs bosons. JHEP **06**, 137 (2015). arXiv:1504.04630 [hep-ph]

147. B. Ananthanarayan, J. Lahiri, P.N. Pandita, Invisible decays of the heavier Higgs boson in the minimal supersymmetric standard model. Phys. Rev. D **91**, 115025 (2015). arXiv:1507.01747 [hep-ph]

148. R.K. Barman, B. Bhattacherjee, A. Chakraborty, A. Choudhury, Study of MSSM heavy Higgs bosons decaying into charginos and neutralinos. Phys. Rev. D **94**(7), 075013 (2016). arXiv:1607.00676 [hep-ph]

149. R.K. Barman, B. Bhattacherjee, A. Choudhury, D. Chowdhury, J. Lahiri, S. Ray, Current status of MSSM Higgs sector with LHC 13 TeV data. arXiv:1608.02573 [hep-ph]

150. E. Arganda, J.L. Díaz-Cruz, N. Mileo, R.A. Morales, A. Szynkman, Search strategies for pair production of heavy Higgs bosons decaying invisibly at the LHC. Nucl. Phys. B **929**, 171–192 (2018). arXiv:1710.07254 [hep-ph]

151. S. Profumo, T. Stefaniak, L. Stephenson, L. Haskins, The not-so-well tempered neutralino. Phys. Rev. D **96**(5), 055018 (2017). arXiv:1706.08537 [hep-ph]

152. A. Aboubrahim, P. Nath, Naturalness, the hyperbolic branch, and prospects for the observation of charged Higgs bosons at high luminosity LHC and 27 TeV LHC. Phys. Rev. D **98**(9), 095024 (2018). arXiv:1810.12868 [hep-ph]

153. S. Gori, Z. Liu, B. Shakya, Heavy Higgs as a portal to the supersymmetric electroweak sector. arXiv:1811.11918 [hep-ph]

154. CMS Collaboration, A.M. Sirunyan et al., Search for electroweak production of charginos and neutralinos in multilepton final states in proton–proton collisions at $\sqrt{s}$ = 13 TeV. JHEP **03**, 166 (2018). arXiv:1709.05406 [hep-ex]

155. CMS Collaboration, A.M. Sirunyan et al., Searches for pair production of charginos and top squarks in final states with two oppositely charged leptons in proton-proton collisions at $\sqrt{s}$ = 13 TeV. JHEP **11**, 079 (2018). arXiv:1807.07799 [hep-ex]

156. CMS Collaboration, A.M. Sirunyan et al., Combined search for electroweak production of charginos and neutralinos in proton-proton collisions at $\sqrt{s}$ = 13 TeV. JHEP **03**, 160 (2018). arXiv:1801.03957 [hep-ex]

157. ATLAS Collaboration, M. Aaboud et al., Search for chargino-neutralino production using recursive jigsaw reconstruction in final states with two or three charged leptons in proton–proton collisions at $\sqrt{s}$ = 13 TeV with the ATLAS detector. Phys. Rev. D **98**(9), 092012 (2018). https://doi.org/10.1103/PhysRevD.98.092012. arXiv:1806.02293 [hep-ex]

158. ATLAS Collaboration, M. Aaboud et al., Search for supersymmetry in events with four or more leptons in $\sqrt{s}$ = 13 TeV pp collisions with ATLAS. Phys. Rev. D **98**(3), 032009 (2018). arXiv:1804.03602 [hep-ex]

159. ATLAS Collaboration, M. Aaboud et al., Search for electroweak production of supersymmetric particles in final states with two or three leptons at $\sqrt{s}$ = 13 TeV with the ATLAS. Eur. Phys. J. C **78**(12), 995 (2018). https://doi.org/10.1140/epjc/s10052-018-6423-7. arXiv:1803.02762 [hep-ex]

160. CMS Collaboration, A.M. Sirunyan et al., Search for new physics in events with two soft oppositely charged leptons and missing transverse momentum in proton-proton collisions at $\sqrt{s}$ = 13 TeV. Phys. Lett. B **782**, 440–467 (2018). arXiv:1801.01846 [hep-ex]

161. ATLAS Collaboration, M. Aaboud et al., Search for electroweak production of supersymmetric states in scenarios with compressed mass spectra at $\sqrt{s}$ = 13 TeV with the ATLAS detector. Phys. Rev. D **97**(5), 052010 (2018). arXiv:1712.08119 [hep-ex]

162. J. Debove, B. Fuks, M. Klasen, Transverse-momentum resummation for gaugino-pair production at hadron colliders. Phys. Lett. B **688**, 208–211 (2010). arXiv:0907.1105 [hep-ph]

163. J. Debove, B. Fuks, M. Klasen, Threshold resummation for gaugino pair production at hadron colliders. Nucl. Phys. B **842**, 51–85 (2011). arXiv:1005.2909 [hep-ph]

164. J. Debove, B. Fuks, M. Klasen, Joint resummation for gaugino pair production at hadron colliders. Nucl. Phys. B **849**, 64–79 (2011). arXiv:1102.4422 [hep-ph]

165. B. Fuks, M. Klasen, D.R. Lamprea, M. Rothering, Gaugino production in proton-proton collisions at a center-of-mass energy of 8 TeV. JHEP **10**, 081 (2012). arXiv:1207.2159 [hep-ph]

166. B. Fuks, M. Klasen, D.R. Lamprea, M. Rothering, Precision predictions for electroweak superpartner production at hadron colliders with Resummino. Eur. Phys. J. C **73**, 2480 (2013). arXiv:1304.0790 [hep-ph]

167. S. Dulat, T.-J. Hou, J. Gao, M. Guzzi, J. Huston, P. Nadolsky, J. Pumplin, C. Schmidt, D. Stump, C.P. Yuan, New parton distribution functions from a global analysis of quantum chromodynamics. Phys. Rev. D **93**(3), 033006 (2016). arXiv:1506.07443 [hep-ph]